

A Solvable Regime of Disorder and Interactions in Ballistic Nanostructures, Part I: Consequences for Coulomb Blockade

Ganpathy Murthy¹, R. Shankar², Damir Herman³, and Harsh Mathur³

¹*Department of Physics and Astronomy, University of Kentucky, Lexington KY 40506-0055*

²*Department of Physics, Yale University, New Haven CT 06520*

³*Physics Department, Case Western Reserve University, Cleveland, OH 44106-7079*

(October 5, 2018)

We provide a framework for analyzing the problem of interacting electrons in a ballistic quantum dot with chaotic boundary conditions within an energy E_T (the Thouless energy) of the Fermi energy. Within this window we show that the interactions can be characterized by Landau Fermi liquid parameters. When g , the dimensionless conductance of the dot, is large, we find that the disordered interacting problem can be solved in a saddle-point approximation which becomes exact as $g \rightarrow \infty$ (as in a large- N theory). The infinite g theory has two phases as a function of the Landau parameter u_m in a channel with angular momentum m : A weak-coupling phase where constant charging and exchange interactions dominate the low-energy physics, as in previous “Universal Hamiltonian” treatments, and a strong-coupling phase characterized by the same order parameter as in the Pomeranchuk transition in clean systems (a spontaneous interaction-induced Fermi surface distortion), but smeared and pinned by disorder. Thus, both interactions and disorder are crucial to the existence of these phases. At finite g , the two phases and critical point evolve into three regimes in the $u_m - 1/g$ plane – weak- and strong-coupling regimes separated by crossover lines from a quantum-critical regime controlled by the quantum critical point. In this, the first of a two part series, we focus on the consequences of this picture for Coulomb Blockade experiments. We employ analytical and numerical methods to predict the statistics of single-particle levels, Coulomb Blockade peak spacings, conductance peak heights and quasiparticle widths. We show that in the strong-coupling and quantum-critical regions, the quasiparticle acquires a width of the same order as the level spacing Δ within a few Δ 's of the Fermi energy due to coupling to collective excitations. In the strong coupling regime if m is odd, the dot will (if isolated) cross over from the orthogonal to unitary ensemble for an exponentially small external flux, or will (if strongly coupled to leads) break time-reversal symmetry spontaneously. For any m , the peak spacing distribution becomes broader than expected in previous works and even has support at negative values, which in turn is correlated with small peak heights. Ballistic/chaotic quantum dots afford us unrivalled theoretical and experimental control over the problem of simultaneous disorder and interactions due to the $1/g$ expansion and our ability to vary disorder and interaction much more readily than in the bulk.

73.50.Jt

I. INTRODUCTION

The problem of treating electronic interactions in mesoscopic systems brings together two very interesting subfields of condensed matter physics. On the one hand, bulk systems with interactions and disorder can show unexpected phenomena¹, and are the subject of ongoing and vigorous investigation. On the other hand, mesoscopic systems² can show behavior which is not present in bulk systems. Two examples are the oscillations as a function of gate voltage V_g in the tunnelling conductance of a quantum dot (QD) weakly coupled to the leads (the Coulomb Blockade (CB) regime³⁻⁷), and persistent currents⁸ in small metallic rings subject to a Aharonov-Bohm flux.

In recent months we have developed a formalism that can tackle the problem of mesoscopic, disordered, strongly correlated systems^{9,10}. We showed that there exists a controlled and complete solution to this problem provided the quantum dot (or ring) is ballistic, meaning that the disorder comes from chaotic collisions with the

walls of the mesoscopic structure, and not from impurities inside it. The solution becomes exact in the limit when the dimensionless conductance g of the quantum dot becomes large^{9,10}. In this paper we focus on the details of our approach in CB regime, while Part II¹¹ of this paper will analyze the effects on persistent currents (a short report of which has appeared¹²). Experimental Coulomb Blockade samples⁵⁻⁷ are ballistic and do have fairly large conductances ($g \approx 5 - 20$). Our predictions are directly applicable to such samples even if the interactions between electrons are strong, which can be achieved by lowering the electron density below that of present samples.

Let us first look at some important length, time, and energy scales to set up the problem. We will confine our analysis to two dimensions, since experimental samples are made by confining a two-dimensional electron gas (2DEG) laterally by means of gates. We will focus attention on ballistic QD's for which the bulk mean free path l is much larger than system size L . Ignoring the (weak) coupling to the leads produces sharp single-particle levels

in the QD whose mean spacing is Δ . A famous conjecture by Bohigas, Giannoni, and Schmidt¹³ states that all levels within a Thouless energy $E_T = \hbar v_F/L$ of each other have correlations controlled by Random Matrix Theory (RMT)¹⁴. The analogous conjecture has been proved for the case of diffusive QD's¹⁵, and there are ongoing efforts to prove it for the ballistic case¹⁶. We will be interested in applying RMT to states that lie within E_T of the Fermi energy. Of particular interest to us are two RMT ensembles¹⁴, the Gaussian Orthogonal Ensemble (GOE) which applies to time-reversal invariant systems, and the Gaussian Unitary Ensemble (GUE) which applies to systems in which time-reversal is broken by an external magnetic flux. We will assume that spin-orbit coupling is negligible throughout this work. Also, because of a variety of factors, the coupling of the external magnetic field to the spin is small compared to the orbital effects in *GaAs*, the standard material used to make quantum dots. To simplify matters, we will set the spin- B -field coupling to zero in what follows. The dimensionless conductance g (also called the Thouless number) is defined by the ratio $g = E_T/\Delta$. Two energies inherited from the bulk 2DEG are the bandwidth E_b and the Fermi energy E_F . The strength of interactions in the bulk 2DEG is characterized by the dimensionless number $r_s = a/a_0$, where $a = 1/\sqrt{\pi\rho}$ is the typical distance between neighboring particles (ρ is the density) while $a_0 = \hbar^2/mc^2$ is the Bohr radius. The band effective mass must be used in computing a_0 as must the dielectric constant. Since the system is finite, capacitive effects produce a charging energy $U_0 = e^2/C$, where C is the capacitance.

The experiments that contributed greatly to our understanding have been on the the zero-bias conductance of a QD weakly coupled to the leads as a function of V_g at $T = 0$. At a generic value of V_g the ground state has a definite number of particles N and energy \mathcal{E}_N . If the chemical potential $\mu = \mathcal{E}_{N+1} - \mathcal{E}_N = \alpha e V_g$ (α is a geometry-dependent ‘‘leverage’’ factor⁴) the free energies of the N and $N + 1$ -particle states are degenerate, and a tunneling peak occurs at zero bias. Successive peaks are separated by the second difference of \mathcal{E}_N , called Δ_2 , the distribution of which is measured^{5,6}.

To analyze the problem theoretically, it is simplest to consider a theory within the Thouless shell around E_F (defined by $|\varepsilon - E_F| \leq E_T/2$). In this shell all the statistical properties of the single-particle energies and wavefunctions can be obtained from RMT. The generic Hamiltonian in this shell can be written as

$$H = \sum_{\alpha} c_{\alpha}^{\dagger} c_{\alpha} \varepsilon_{\alpha} + \frac{1}{2} \sum_{\alpha\beta\gamma\delta} V_{\alpha\beta\gamma\delta} c_{\alpha}^{\dagger} c_{\beta}^{\dagger} c_{\gamma} c_{\delta} \quad (1)$$

where ε_{α} are single-particle levels that obey RMT statistics, have a mean spacing Δ and range from $-g\Delta/2$ to $g\Delta/2$, and $V_{\alpha\beta\gamma\delta}$ represents a two-body interaction. In the following we will suppress spin for simplicity, pointing out how its restoration modifies various results. Different forms of $V_{\alpha\beta\gamma\delta}$ turn out to represent very different physics.

The simplest model for interactions in a QD has a constant charging energy^{3,4} U_0 :

$$H_U = \sum_{\alpha,s} \varepsilon_{\alpha} c_{\alpha,s}^{\dagger} c_{\alpha,s} + \frac{U_0}{2} \hat{N}^2 \quad (2)$$

which corresponds to the choice $V_{\alpha\beta\gamma\delta} = U_0 \equiv u_0 \Delta$, (independent of α and β with all other couplings not of this form vanishing). This model predicts a bimodal distribution for Δ_2 : Adding an electron above a doubly-filled (spin-degenerate) level costs $U_0 + \varepsilon$, with ε being the energy to the next single-particle level. Adding it to a singly occupied level costs U_0 . While the second contribution gives a Dirac delta-function peak at U_0 , the first contribution is the distribution of nearest neighbor level separation ε , which is known¹⁴ from RMT to have a width of the order of the mean single-particle level spacing Δ . The puzzle that stimulated recent theoretical developments in the field is that numerics^{17,18} and experiments^{5,6} produce distributions for Δ_2 which do not show any bimodality, and are much broader.

One interesting option is to consider $V_{\alpha\beta\gamma\delta}$ as independent gaussian variables¹⁹. Our work is more closely related to another, the Universal Hamiltonian^{20,21}, wherein (for the spinful case) a term coupling to total \vec{S}^2 and a Cooper coupling also appear:

$$H_U = \sum_{\alpha,s} \varepsilon_{\alpha} c_{\alpha,s}^{\dagger} c_{\alpha,s} + \frac{U_0}{2} \hat{N}^2 - \frac{J}{2} \vec{S}^2 + \lambda \left(\sum_{\alpha} c_{\alpha,\uparrow}^{\dagger} c_{\alpha,\downarrow}^{\dagger} \right) \left(\sum_{\beta} c_{\beta,\downarrow} c_{\beta,\uparrow} \right) \quad (3)$$

The rationale for the above choice of interactions is the following: As we will see below, only the ‘‘diagonal’’ matrix elements in which the indices are pairwise equal survive the ensemble average and the variances of all the matrix elements are small

$$\langle V_{\alpha\beta\gamma\delta}^2 \rangle - \langle V_{\alpha\beta\gamma\delta} \rangle^2 \simeq \frac{\Delta^2}{g^2} \quad (4)$$

where the indices now describe orbital and spin variables. Thus for large g , the interaction may be approximated by its ensemble average, which is just the Universal Hamiltonian. Apart from this motivation, calculations based on the Universal Hamiltonian^{20,21} have proven very successful at describing experiments⁵ on quantum dots with small $r_s \approx 1$ at a quantitative level, once experimental noise is subtracted out and finite-temperature effects^{22–24} are taken into account.

Our work deals with situations where r_s is a lot larger than in current samples, in which case other unexpected phenomena appear possible. Our choice of $V_{\alpha\beta\gamma\delta}$ follows from the assumption of Landau Fermi liquid interactions at the Thouless energy^{9,10}, which we justify using renormalization group arguments. The Landau interactions^{25,26} are parametrized by couplings u_m in every angular momentum channel m . For the spinful case the set of parameters is doubled, with one for the charge and one for the spin. Keeping only u_0^{charge} and u_0^{spin} yields the Universal Hamiltonian (without the Cooper term). The retention of all the Landau parameters leads to the emergence of strong-coupling regimes in $m \neq 0$

angular momentum channels^{9,10}, which exhibit a spontaneous deformation of the Fermi surface (suitably smeared out and pinned by disorder) as well as the possibility of time-reversal violation. The transition was originally discovered in the clean bulk limit by Pomeranchuk²⁷. While these are true second-order quantum phase transitions in the limit $g \rightarrow \infty$, they are replaced by sharp crossovers for finite but large g . This paper presents in detail the physics of these new phases, the transitions/crossovers between the weak- and strong-coupling regime via the quantum-critical regime and their attendant signatures. We concentrate on charge-channel instabilities in the spinful system; spin-channel instabilities necessarily involve the exchange coupling J and will be the subject of future work. The purpose of this set of two papers is to supply all the details left out of the previous brief presentations^{9,10,12}, as well as to present numerical corroboration of the earlier analytical results, many new results, and experimental signatures.

The plan of the paper is as follows. In section II we present the renormalization group (RG) argument²⁸ for starting with Landau Fermi liquid interactions in the Thouless band, with all the assumptions and caveats. In particular, we will show why these assumptions are reasonable for ballistic QD's but might fail for QD's deep in the diffusive limit²⁹. In Section III we present a further RG analysis inside the Thouless shell (modeled after Ref.³⁰), this time integrating out exact eigenstates of the disordered single-particle Hamiltonian. To leading order in $1/g$ we will see that the RG flow to one-loop order implies the phase transitions mentioned above. However, some questions about the effects of higher loops are left open, as is the very nature of the strong-coupling phase. These issues are resolved in Section IV, where we show that the problem can be mapped on to a large- N theory, with g playing the role of N . * The largeness of g allows us to fully control the calculation at at strong-coupling and not only confirm the phase transition discovered in perturbative RG⁹ but also to probe the strong coupling phase in considerable detail¹⁰. In the next and longest section (Section V) we explore the physical consequences of the large- g solution: The nature of the order parameter, the physical signatures of the strong-coupling regime and the crossover quantum-critical regime³¹, and some curious properties of the weak-coupling regime. Numerical methods which are capable of accessing all regions of the phase diagram (except the quantum critical regime) corroborate the analytical methods and also complement them, for example in the computation of level statistics and the CB peak-spacing statistics in the strong-coupling regime.

We predict that if the system is in the strong-coupling

*This large- N nature has two manifestations, one which is best expressed by saying that a certain class of diagrams dominate over others, and another in which a large number (here g^2) appears in front of the effective action, showing that the saddle-point approximation is a good one.

regime of an even m channel it will display a broadening of the CB peak spacing distribution, correlations between small peak-heights and small peak-spacings, and a diamagnetic persistent current (which is not expected theoretically^{32,33} in non-superconducting materials, but is seen experimentally⁸).

In the strong-coupling regime of an odd m channel, in addition to all the above effects (but with a paramagnetic persistent current), the system can be mapped on to the Caldeira-Leggett³⁴ model of a particle in a double-well potential subject to ohmic dissipation. The solution to this model^{35,36} shows that the m odd system can be driven through a quantum phase transition which spontaneously breaks time-reversal symmetry by changing the coupling of the quantum dot to the leads. (This really is a phase transition since the quantum coherence of the dot with the infinite reservoir renders a sharp transition possible).

In this section we will also show that while an effective single-particle description works in the weak-coupling regime, it fails in the quantum-critical and strong-coupling regimes even at low energies of order a few Δ . In these latter regions we will make a connection to ideas of ‘‘Fock-space localization/delocalization’’^{37,38}, which captures the crossover of the spectral width of the quasiparticle to a Breit-Wigner form as the quasiparticle energy is increased. This long section ends with its own summary. In Section VI our conclusions are presented, as are discussions of how our approach might be useful in other problems involving disorder and interactions. Appendices A and B contain some additional details.

II. EFFECTIVE INTERACTIONS AT THE THOULESS ENERGY

In this section we will give a brief introduction to Fermi liquid theory^{25,26} in the bulk, describe its instabilities²⁷, and see how it must be modified to account for disorder. We will argue that a hybrid Hamiltonian, with a single-particle part encoding the chaotic nature of the single-particle states, and a part with Fermi liquid interactions, is the most natural starting point for analyzing ballistic mesoscopic structures in the Thouless band.

A. The Clean Limit in the Bulk

It is well-known that in a clean two-dimensional bulk system, no matter what interactions one starts with in the bare Hamiltonian, provided no superconducting or density wave instabilities intervene, the effective interactions are of the Landau Fermi liquid form^{25,26,28} in a sufficiently thin shell near the Fermi surface defined by $|\mathbf{k}| - k_F \leq k_{max}$. This corresponds to an energy cutoff $\Lambda = v_F k_{max}$. The entire Hamiltonian in such a thin shell can be written for the spinless case as

$$H_{FL} = \sum_{\mathbf{k}} \varepsilon_0(\mathbf{k}) c^\dagger(\mathbf{k}) c(\mathbf{k}) + \frac{1}{2N_0} \sum_{\mathbf{k}, \mathbf{k}', \mathbf{q}} u(\theta - \theta')$$

$$\times : c^\dagger(\mathbf{k} - \mathbf{q})c(\mathbf{k})c^\dagger(\mathbf{k}' + \mathbf{q})c(\mathbf{k}') : \quad (5)$$

where $\varepsilon_0(\mathbf{k})$ is the renormalized quasiparticle energy measured from the Fermi surface, $c(\mathbf{k})$, $c^\dagger(\mathbf{k})$ are canonical anticommuting fermion operators, N_0 is the single-particle density of states, the $::$ sign stands for normal-ordering (subtracting the average in the ground state), θ , θ' are the angles of the two-dimensional vectors \mathbf{k} , \mathbf{k}' , and $u(\theta - \theta')$ is the (dimensionless) Fermi liquid interaction function. It is understood that \mathbf{k} , \mathbf{k}' are to be summed only over states in the shell, and that $|\mathbf{q}| \leq k_{max}$. The main features of the Fermi liquid interaction are that $u(\theta - \theta')$ does not depend on the radial magnitudes of \mathbf{k} , \mathbf{k}' but only on the angles, and that the interaction shows mostly forward scattering. Rotational invariance has been used to express u as a function of the difference of the angles. One then Fourier decomposes u to obtain

$$u(\theta - \theta') = u_0 + \sum_{m=1}^{\infty} u_m \cos m(\theta - \theta') \quad (6)$$

where the u_m are known as Landau parameters. The Fermi liquid interaction function also determines the energy to add a quasiparticle with momentum \mathbf{k} in the presence of a background of excited quasiparticles/quasihilos specified by $\delta n(\mathbf{k}')$ (which is the deviation in occupation from the ground state)

$$\varepsilon(\mathbf{k}) = \varepsilon_0(\mathbf{k}) + \frac{1}{N_0} \sum_{\mathbf{k}'} u(\theta - \theta') \delta n(\mathbf{k}') \quad (7)$$

and the Landau total energy functional

$$\mathcal{E}(\{\delta n\}) = \sum_{\mathbf{k}} \varepsilon_0(\mathbf{k}) \delta n(\mathbf{k}) + \frac{1}{2N_0} \sum_{\mathbf{k}\mathbf{k}'} u(\theta - \theta') \delta n(\mathbf{k}) \delta n(\mathbf{k}') \quad (8)$$

Landau's original derivation^{25,26} rests on phase space and adiabatic continuity arguments and also predicts a decay rate for quasiparticles of order ε^2/E_F , which has been neglected above. The same result can also be derived by integrating out high energy states (single-particle states far from the Fermi surface) in a renormalization group (RG) approach, as was shown by one of us a decade ago²⁸. In this approach, at a given stage of the RG one has a theory with a certain cutoff k_{max} . One then integrates out a thin "shell" of momenta or width δk_{max} , thereby obtaining an effective theory with a cutoff $k_{max} - \delta k_{max}$. One demands that the new theory give the same answer for all physical Green's functions in the low-energy sector as the theory with cutoff k_{max} . To achieve this the coupling constants must flow as one changes the cutoff. If a certain coupling constant increases as high-energy states are integrated out, it will end up dominating the low-energy physics no matter how small it was initially. Such a coupling is called "relevant". In the opposite case a coupling may shrink as high-energy states are integrated out, in which case it is unimportant for low-energy physics, and is called "irrelevant". Couplings which do not flow are called "marginal". It turns

out that all the Landau parameters are marginal for a clean system in the bulk, whereas all other types of couplings, with one exception are irrelevant. The exception is the coupling in the BCS channel, i.e., between particle of opposite momenta. These are irrelevant if repulsive and relevant if attractive. Since no superconductivity has ever been detected in the *GaAs* 2DEG's which are the basis of the ballistic quantum dots we focus on, we will assume that the BCS instability is absent.

Thus, the Landau theory defines a fixed point (in fact a whole class of fixed points) for the clean electron gas.

B. Fermi Liquid Parameters for the Spinful Case

In the spinful case the Fermi liquid interaction function is to be thought of as a matrix in spin space²⁶. Consider the energy to add a particle in a momentum state \mathbf{k} with a density matrix $\rho_{ss'}(\mathbf{k})$. This energy is

$$\varepsilon_{\{\rho\}}(\mathbf{k}) = Tr(\varepsilon(\mathbf{k})\rho(\mathbf{k})) = \sum_{ss'} \varepsilon_{ss'} \rho_{s's} \quad (9)$$

The energy matrix $\varepsilon_{ss'}(\mathbf{k})$ depends on the occupations and spin states of other quasiparticles, or in other words, the density matrices $\delta n_{s_1 s'_1}(\mathbf{k}')$ in the following way

$$\varepsilon_{ss'}(\mathbf{k}) = \varepsilon_{0,ss'}(\mathbf{k}) + \frac{1}{N_0} \sum_{s_1 s'_1, \mathbf{k}\mathbf{k}'} u_{ss', s_1 s'_1}(\theta - \theta') \delta n_{s_1 s'_1}(\mathbf{k}') \quad (10)$$

with the corresponding total energy functional

$$\mathcal{E}(\{\delta n\}) = \sum_{ss'\mathbf{k}} \varepsilon_{0,ss'}(\mathbf{k}) \delta n_{s's}(\mathbf{k}) + \frac{1}{2N_0} \sum_{ss' s_1 s'_1, \mathbf{k}\mathbf{k}'} u_{ss', s_1 s'_1}(\theta - \theta') \delta n_{ss'}(\mathbf{k}) \delta n_{s_1 s'_1}(\mathbf{k}') \quad (11)$$

We will restrict ourselves to the case with spin-rotation-invariance, which leads to a restricted form for the interaction function²⁶

$$u_{ss', s_1 s'_1}(\theta - \theta') = \Phi(\theta - \theta') \delta_{ss'} \delta_{s_1 s'_1} + Z(\theta - \theta') \vec{\tau}_{ss'} \cdot \vec{\tau}_{s_1 s'_1} \quad (12)$$

where the $\vec{\tau} = (\tau^{(x)}, \tau^{(y)}, \tau^{(z)})$ are the Pauli spin matrices, and the Φ and Z are the Fermi liquid interaction functions in the charge and spin channels respectively. As usual, these can be Fourier expanded to obtain the charge and spin channel Landau parameters

$$\Phi(\theta - \theta') = \Phi_0 + \sum_{m=1}^{\infty} \Phi_m \cos m(\theta - \theta') \quad (13)$$

$$Z(\theta - \theta') = Z_0 + \sum_{m=1}^{\infty} Z_m \cos m(\theta - \theta') \quad (14)$$

The Φ_m and Z_m are identical to the parameters used by Pines and Nozieres⁴¹,

$$F_m^s = \Phi_m \quad (15)$$

$$F_m^a = Z_m \quad (16)$$

The Landau parameters depend on the relative strength of the interaction and kinetic energies, commonly characterized by the dimensionless number $r_s = a/a_0$, where $a = 1/\sqrt{\pi\rho}$ is the typical distance between neighboring particles (ρ is the density) while $a_0 = \hbar^2/me^2$ is the Bohr radius. The band effective mass must be used in computing a_0 as must the dielectric constant. The dependence of the Landau parameters on r_s has been the subject of investigation by quantum Monte Carlo methods⁴². For the largest value investigated $r_s = 5$, the results in our normalization (differing from that of ref.⁴² by a factor of two) are

$$\Phi_0 = -1.85 \quad (17)$$

$$Z_0 = -0.25 \quad (18)$$

$$\Phi_1 = 0.06 \quad (19)$$

$$Z_1 = -0.135 \quad (20)$$

$$\Phi_2 = -0.25 \quad (21)$$

$$Z_2 = 0.16 \quad (22)$$

C. Instabilities of the Clean Fermi Liquid

It is well-known that the Fermi liquid is unstable towards the introduction of an attractive coupling in the Cooper channel which leads to a gapped superconducting ground state. The Fermi liquid also has other instabilities for certain values of the Fermi liquid parameters, a fact first pointed out by Pomeranchuk²⁷. There has been a revival of interest in the Pomeranchuk transition in clean bulk 2D systems recently^{43,44}.

Let us first consider the spinless case. We consider a deformation of the Fermi surface by an amount $r(\theta)$ in the direction θ . To be precise, we consider the following deformation

$$\delta n(\mathbf{k}) = \begin{cases} 1, & 0 \leq \varepsilon_0(\mathbf{k}) \leq r(\theta), \quad r \geq 0 \\ -1, & r(\theta) \leq \varepsilon_0(\mathbf{k}) \leq 0, \quad r \leq 0 \end{cases} \quad (23)$$

Using the replacement $\sum_{\mathbf{k}} \rightarrow N_0 \int d\varepsilon$ we can calculate the energy cost for this deformation using the Landau energy functional, Eq. (8),

$$\frac{\mathcal{E}}{N_0} = \int_0^{2\pi} \frac{d\theta}{2\pi} \frac{r(\theta)^2}{2} + \frac{1}{2} \int_0^{2\pi} \frac{d\theta d\theta'}{(2\pi)^2} u(\theta - \theta') r(\theta) r(\theta') \quad (24)$$

To isolate a particular Fermi liquid channel of angular momentum $m \neq 0$ we choose $r(\theta) = r_0 \cos m\theta$ to obtain the total energy for $m \neq 0$

$$\frac{\mathcal{E}}{N_0} = \frac{r_0^2}{4} (1 + u_m/2) \quad (25)$$

It is clear that for $u_m \leq -2$ the energy is negative, indicating an instability of the undeformed Fermi liquid. This is the Pomeranchuk instability²⁷.

In the spinful case the “deformation” can be in the charge or the spin channel. Let us consider the instability

in the spin channel for illustration. Now δn must be a density matrix in spin space, and we can choose, for example,

$$\delta n(\mathbf{k}) = \begin{cases} \tau^z, & 0 \leq \varepsilon_0(\mathbf{k}) \leq r(\theta), \quad r \geq 0 \\ -\tau^z, & r(\theta) \leq \varepsilon_0(\mathbf{k}) \leq 0, \quad r \leq 0 \end{cases} \quad (26)$$

Working through the energy functional of Eq. (11) in the same way as before one obtains for $m \neq 0$

$$\frac{\mathcal{E}}{N_0} = \frac{r_0^2}{4} (1 + Z_m) \quad (27)$$

where the extra factor of two inside the brackets compared to Eq. (25) comes from the extra trace over the two-dimensional spin space, combined with the fact that in our normalization, N_0 is the *spinless* single-particle density of states. Thus, in the spinful case, with our normalizations, the instability occurs for $\Phi_m, Z_m \leq -1$. From the values quoted⁴² in the last section, we see that the electron gas in the clean bulk limit is quite far from these instabilities even for $r_s = 5$.

D. The Disordered Bulk

Let us now examine the changes that occur when elastic impurity scattering is taken into account in the bulk. The RG method can be conceptually generalized for this case as well. An important energy scale here is $E_\tau = \hbar/\tau = \hbar v_F/l$, where l is the mean free path due to impurities and τ the mean free time. In a time-scale τ momentum states get scattered by impurities implying that E_τ is the spectral broadening of a momentum state. Since impurity scattering is elastic, an exact eigenstate of the disordered single-particle Hamiltonian with energy ε can be expressed as a superposition of momentum states of energy ε with a spread of E_τ . Therefore for high energies $\varepsilon \gg E_\tau$ integrating out a momentum states of thickness E_τ is roughly the same as integrating out a corresponding shell of exact energy eigenstates. This is equivalent to the statement that states of high energy have negligible correlations with low-energy states.

One can now ask how the interaction coupling constants flow in the disordered case. Consider first the case of a microscopic short-ranged interaction of range ξ , such as in He^3 . The time taken by a single fermion-fermion collision is then roughly ξ/v_F . As long as this time is much smaller than τ , the collisions happen far from an impurity, and therefore conserve total momentum. Thus, despite the fact that momentum is not a good quantum number for single-particle states, interactions continue to conserve momentum. Since integrating out momentum states is roughly the same as integrating out exact energy eigenstates, the conclusion is that up to an energy cutoff Λ of the order of magnitude of E_τ the RG flow should proceed much as in the clean system, resulting in Fermi liquid interactions.

Once the cutoff reaches E_τ integrating out momentum states is no longer approximately equivalent to integrating out exact eigenstates of the disordered single-particle Hamiltonian, since now the wavefunctions of the

states being integrated out have non-negligible correlations (induced by disorder) with states being kept. In the disorder-averaged version of the theory^{45,46}, these correlations manifest themselves as collective modes such as diffusons and Cooperons with singular propagators. In the diffusive limit, these propagators drive the RG flow^{45,46}, resulting in a runaway flow of the s -wave triplet coupling Z_0 towards strong coupling. The resulting state seems to be weakly ferromagnetic⁴⁷, but is currently not fully understood.

Now consider a model with Coulomb interactions. Up to an energy scale of E_τ a good model for the effective interactions is the Thomas-Fermi static screened interaction $v_{TF}(q) = 2\pi e^2/(q + q_{TF})$, with a screening wavevector $q_{TF} \approx a_0^{-1}$ in two dimensions (a_0 is the effective Bohr radius in the material). By following the previous logic, it is clear that as long as $1/q_{TF}l$ is small, electron-electron collisions will conserve total momentum, leading to Fermi liquid interactions near E_F . However, at very low energies, deep in the diffusive regime ($\omega\tau \ll 1$, $ql \ll 1$) this interaction can get unscreened²⁹. The resulting low-energy unscreened interaction leads to a breakdown of Fermi liquid theory in two dimensions at the most fundamental level, namely, the quasiparticle lifetime broadening becomes comparable to its energy²⁹. It is also clear that in this regime, the electron-electron collision time is long compared to τ , and therefore momentum will not be conserved in an electron-electron collision.

E. Ballistic Quantum Dots

Now let us examine the case of ballistic QD's, which is conceptually the same as considering electrons in a cavity with hard walls. Here since the role of impurity scattering is being played by scattering from the walls of the cavity, L plays the role of l . Therefore the Thouless scale E_T is roughly the same as E_τ . Since we know that the interaction is screened at this energy scale, we can conclude that Fermi liquid interactions are valid at this scale. Can Fermi liquid interactions become invalid at lower energies due to Altshuler-Aronov-like effects²⁹? The answer is no: Due to the finite size of the cavity, all momenta can only be defined up to an uncertainty of $2\pi/L$. Since q can only be defined up to order $1/L$, one can never achieve the condition $qL \ll 1$. The deep diffusive regime where interactions get unscreened is inaccessible in ballistic QD's, and is superceded by the Random Matrix (RMT) regime which we will analyze in detail in the next section. The conclusion of this set of arguments is that Fermi liquid interactions are natural for ballistic QD's, while they may not be for strongly diffusive ($l \ll L$) QD's.

Let us now explicitly consider what the low-energy effective Hamiltonian looks like for a ballistic QD in the Thouless band. We will first write it down, and then discuss it.

$$H = \sum_{\alpha} \varepsilon_{\alpha} c_{\alpha}^{\dagger} c_{\alpha} + \frac{\Delta}{2} \sum_{\mathbf{k}, \mathbf{k}'} u(\theta - \theta') : n_{\mathbf{k}} n_{\mathbf{k}'} : \quad (28)$$

where α are labels for the exact eigenstates (g in number) of the single-quasiparticle Hamiltonian encoding the chaotic boundary scattering, Δ (the mean level spacing) is the inverse density of spinless states $1/N_0$, $n_{\mathbf{k}} = c^{\dagger}(\mathbf{k})c(\mathbf{k})$, and it is understood that the sum over \mathbf{k} , \mathbf{k}' goes over g values near the Fermi surface. (We are using $n_{\mathbf{k}}$ instead of $\delta n_{\mathbf{k}}$, the difference being absorbed in a shift in the chemical potential.) The Hamiltonian is expressed in a hybrid basis, with the connection between the α and the \mathbf{k} basis being given by the wavefunctions of the exact eigenstates α in the momentum basis $\phi_{\alpha}(\mathbf{k})$. The statistics of the energies ε_{α} and wavefunctions $\phi_{\alpha}(\mathbf{k})$ are assumed to be controlled by RMT. Note that the momentum \mathbf{k} is uncertain up to $2\pi/L$, and it really represents a patch on the Fermi surface. To be more precise, we can define the state we label by \mathbf{k} in the dot as

$$|\mathbf{k}\rangle = \sum_{\alpha} |\alpha\rangle \langle \alpha| e^{i\mathbf{k}\cdot\mathbf{r}} = \sum_{\alpha} |\alpha\rangle \phi_{\alpha}(\mathbf{k}) \quad (29)$$

For convenience we will choose the \mathbf{k} labels to be equally spaced (separated by an angle $2\pi/k_F L = 2\pi/g$) on the Fermi circle. This set of states clearly satisfies all the boundary conditions of the dot, and is unitarily related to the set of disorder eigenstates $|\alpha\rangle$. In the original Fermi liquid Hamiltonian (Eq. (5)) there was an additional sum over \mathbf{q} . Here, since \mathbf{q} is also uncertain up to $2\pi/L$ and only scattering within the Thouless shell is allowed, the sum over \mathbf{q} is eliminated. Since the \mathbf{k} take on g discrete values, Landau parameters with angular momentum m of order g are not sensible in this theory. Our focus will be on small m of order 1, because these are the channels in which the Landau parameters are expected to have large magnitudes.

An interesting fact about ballistic/chaotic quantum dots is that the ratio E_F/E_T is related to g :

$$\frac{E_F}{E_T} = \frac{\hbar^2 k_F^2 / 2m^*}{\hbar v_F / L} = \frac{k_F L}{2} \simeq g \quad (30)$$

Recall that Fermi liquid theory becomes applicable only in an energy shell of size much smaller than E_F around the Fermi surface. Therefore the largeness of g is also a sufficient condition for the validity of the Fermi liquid interactions.

To summarize, in writing down the Hamiltonian of Eq. (28), we are appealing to the fact that whereas single particle momentum is not conserved due to collision with the walls, the momentum of a pair is conserved during a collision if it takes place over a time scale shorter than L/v_F , the time to bounce off the wall. The interacting part of the Hamiltonian continues to have the same form as in the clean limit even in the presence of chaotic boundary scattering.

F. Recovering the Universal Hamiltonian

Let us see how the Universal hamiltonian of Eqn. (3) emerges, starting with the spinless case. One can use the

$\phi_\alpha(\mathbf{k})$ to express the entire Hamiltonian in the α basis in the form of Eq. (1), with

$$V_{\alpha\beta\gamma\delta} = \frac{\Delta}{4} \sum_{\mathbf{k}\mathbf{k}'} u(\theta - \theta') \left[\phi_\alpha^*(\mathbf{k})\phi_\beta^*(\mathbf{k}') - \phi_\alpha^*(\mathbf{k}')\phi_\beta^*(\mathbf{k}) \right] \times [\phi_\gamma(\mathbf{k}')\phi_\delta(\mathbf{k}) - \phi_\gamma(\mathbf{k})\phi_\delta(\mathbf{k}')] \quad (31)$$

These coefficients $V_{\alpha\beta\gamma\delta}$ will vary from sample to sample. Let us focus on terms that survive the ensemble average, which here reduces to a Random Matrix Theory¹⁴ average. Let us concentrate on the GOE, where all the wavefunctions in the real-space basis $\phi_\alpha(\mathbf{r})$ can be made real. Since we are working in an approximate momentum basis labeled by the g values of \mathbf{k} , the reality of the real-space wavefunctions translates to

$$(\phi_\alpha(\mathbf{k}))^* = \phi_\alpha(-\mathbf{k}) \quad (32)$$

The fundamental RMT wavefunction correlator is¹⁴

$$\langle \phi_\alpha^*(\mathbf{k})\phi_\beta(\mathbf{k}') \rangle = \frac{\delta_{\alpha\beta}\delta_{\mathbf{k}\mathbf{k}'}}{g} \quad (33)$$

To find the average of $V_{\alpha\beta\gamma\delta}$ we need the four-point correlator. Apart from exceptional cases when all the subscripts and/or all the arguments of the wavefunctions are equal, the four-point wavefunction correlator in the GOE can be written to leading order in $1/g$ as

$$\langle \phi_\alpha^*(\mathbf{k}_1)\phi_\beta^*(\mathbf{k}_2)\phi_\gamma(\mathbf{k}_3)\phi_\delta(\mathbf{k}_4) \rangle = \frac{\delta_{\alpha\delta}\delta_{\beta\gamma}\delta_{\mathbf{k}_1\mathbf{k}_4}\delta_{\mathbf{k}_2\mathbf{k}_3}}{g^2} + \frac{\delta_{\alpha\gamma}\delta_{\beta\delta}\delta_{\mathbf{k}_1\mathbf{k}_3}\delta_{\mathbf{k}_2\mathbf{k}_4}}{g^2} + \frac{\delta_{\alpha\beta}\delta_{\gamma\delta}\delta_{\mathbf{k}_1,-\mathbf{k}_2}\delta_{\mathbf{k}_3,-\mathbf{k}_4}}{g^2} \quad (34)$$

It is seen that only matrix elements in which the indices $\alpha\beta\gamma\delta$ are pairwise equal survive disorder-averaging, and also that the average has no dependence on the energy of $\alpha\beta\gamma\delta$. In the spinless case, the first two terms on the right hand side make equal contributions and produce the constant charging energy in the Universal Hamiltonian of Eq. (3), while in the spinful case (to be discussed at length in Section III B) they produce the charging and exchange terms. The final term of Eq. (34) produces the Cooper interaction of Eq. (3).

Finally, one can explicitly calculate the variances

$$\langle V_{\alpha\beta\gamma\delta}^2 \rangle - \langle V_{\alpha\beta\gamma\delta} \rangle^2 = \frac{\Delta^2}{4g^2} \sum_{m=1}^2 u_m^2. \quad (35)$$

and see that they are small. Note that u_0 does not contribute to the fluctuations between different disorder realizations.

III. INSTABILITIES OF THE UNIVERSAL HAMILTONIAN: RENORMALIZATION GROUP TREATMENT

The Universal Hamiltonian^{20,21} is obtained by replacing the interaction by its ensemble average in the full Hamiltonian, arguing that sample-to-sample fluctuations

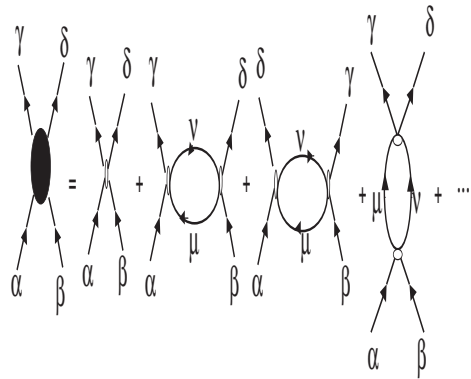


FIG. 1. Feynman diagrams for the full four-point amplitude $\Gamma_{\alpha\beta\gamma\delta}$.

in the interaction matrix elements are small. At this point one can ask when small terms in the Hamiltonian can be safely discarded, and when they cannot⁹. As long as one is interested in low-energy properties, the RG is the perfect tool to answer this question. One simply integrates out high energy states, and looks at the fate of the originally small couplings. If they are irrelevant in the RG sense, discarding them is justified, while if they are relevant they dominate the low-energy physics regardless of how small they were initially.

Two of us carried out just such an RG analysis⁹, to the presentation of which this section is devoted. We will first consider the spinless case, and then make some remarks about the spinful case. We will close this section with a list of questions left unanswered by the RG.

A. RG for the Spinless Case

We start with the Hamiltonian for spinless fermions in a ballistic QD, Eq. (28), which we reproduce here for convenience

$$H = \sum_{\alpha} \varepsilon_{\alpha} c_{\alpha}^{\dagger} c_{\alpha} + \frac{\Delta}{2} \sum_{\mathbf{k}, \mathbf{k}'} u(\theta - \theta') : n_{\mathbf{k}} n_{\mathbf{k}'} : \quad (36)$$

The strategy for carrying out RG in a finite system³⁰ is the following: (i) Since we are in the Thouless shell we cannot integrate out momenta, but must integrate out exact eigenstates of the chaotic single-particle Hamiltonian. (ii) After integrating out some exact eigenstates at a given stage in the RG we have $g' = ge^{-\xi}$ levels left (here ξ is called the flow parameter of the RG). At this stage we compute a scattering amplitude $\Gamma_{\alpha\beta\gamma\delta}$ for the process in which two fermions originally in states $\alpha\beta$ are scattered into states $\gamma\delta$. This scattering can proceed directly through the vertex $V_{\alpha\beta\gamma\delta}(\xi)$, or via intermediate virtual states higher order in the interactions, which can be classified by a set of Feynman diagrams, as shown in Figure 1. All the states in the diagrams belong to the g' states kept. (iii) We demand that the entire amplitude be independent of g' , meaning that the physical amplitudes

should be the same in the effective theory as in the original theory. This will lead to a set of flow equations for the $V_{\alpha\beta\gamma\delta}$. In principle this flow equation will involve all powers of V but we will keep only quadratic terms (the one-loop approximation). Then the diagrams are limited to the ones shown in Figure 1, leading to the following contributions to the scattering amplitude $\Gamma_{\alpha\beta\gamma\delta}$

$$\begin{aligned} \Gamma_{\alpha\beta\gamma\delta} = & V_{\alpha\beta\gamma\delta} \\ & + \sum'_{\mu,\nu} \frac{N_F(\nu) - N_F(\mu)}{\varepsilon_\mu - \varepsilon_\nu} (V_{\alpha\nu\mu\delta} V_{\beta\mu\nu\gamma} - V_{\alpha\nu\mu\gamma} V_{\beta\mu\nu\delta}) \\ & - \sum'_{\mu\nu} \frac{1 - N_F(\mu) - N_F(\nu)}{\varepsilon_\mu + \varepsilon_\nu} V_{\alpha\beta\mu\nu} V_{\nu\mu\gamma\delta} \end{aligned} \quad (37)$$

where the prime on the sum reminds us that only the g' remaining states are to be kept and $N_F(\alpha)$ is the Fermi occupation of the state α . We will confine ourselves to zero temperature where this number can only be zero or one, but the extension to finite temperature is straightforward. Also recall that the matrix element $V_{\alpha\beta\gamma\delta}$ now explicitly depends on the RG flow parameter ξ .

Now we demand that upon integrating the two states at $\pm g'\Delta/2$ we recover the same $\Gamma_{\alpha\beta\gamma\delta}$. Clearly, since $g' = ge^{-\xi}$,

$$\frac{d}{d\xi} = -g' \frac{\delta}{\delta g'} \quad (38)$$

The effect of this differentiation on the loop diagrams is to fix one of the internal lines of the loop to be at the cutoff $\pm g'\Delta/2$, while the other one ranges over all smaller values of energy. In the particle-hole diagram, since μ or ν can be at $+g'\Delta/2$ or $-g'\Delta/2$, and the resulting summations are the same in all four cases, we take a single contribution and multiply by a factor of 4. The same reasoning applies to the Cooper diagram. Let us define the energy cutoff $\Lambda = g'\Delta/2$ to make the notation simpler. Since we are integrating out two states we have $\delta g' = 2$

$$\begin{aligned} 0 = & \frac{dV_{\alpha\beta\gamma\delta}}{d\xi} \\ & - \frac{g'}{2} 4 \sum_{\mu=\Lambda,\nu} \frac{N_F(\nu) - N_F(\mu)}{\varepsilon_\mu - \varepsilon_\nu} (V_{\alpha\nu\mu\delta} V_{\beta\mu\nu\gamma} - V_{\alpha\nu\mu\gamma} V_{\beta\mu\nu\delta}) \\ & + \frac{g'}{2} 4 \sum_{\mu=\Lambda,\nu} \frac{1 - N_F(\mu) - N_F(\nu)}{\varepsilon_\mu + \varepsilon_\nu} V_{\alpha\beta\mu\nu} V_{\nu\mu\gamma\delta} \end{aligned} \quad (39)$$

The changed sign in front of the 1-loop diagrams reflects the sign of Eq. (38)

So far we have not made any assumptions about the form of $V_{\alpha\beta\gamma\delta}$, and the formulation applies to any finite system. In a generic system such as an atom³⁰, the matrix elements depend very strongly on the state being integrated over, and the flow must be followed numerically for each different set $\alpha\beta\gamma\delta$ kept in the low-energy subspace. The crucial simplification in QD's comes from the fact that these matrix elements are random and controlled by RMT, and that the *RG equation is self-averaging*, as will be seen below.

Let us go back to the properly antisymmetrized matrix element defined in terms of the Fermi liquid interaction

function, Eq. (31). Since there is a product of two V 's in each loop diagram, and each V contains 4 terms, it is clear that each loop contribution has 16 terms. However, it turns out that only certain terms contribute to leading order in the large- g limit, while others do not. We will focus on one of each type to illustrate the difference. Let us first consider a term of type I in the particle-hole diagram, which survives in the large- g limit. Putting in the full wavefunction dependences (and ignoring factors other than g, g') we have

$$\begin{aligned} & g' \Delta^2 \sum_{\nu=-\Lambda}^0 \frac{1}{\Lambda + |\varepsilon_\nu|} \\ & \sum_{\mathbf{k}\mathbf{k}'} \sum_{\mathbf{p}\mathbf{p}'} u(\theta_{\mathbf{k}} - \theta_{\mathbf{p}}) u(\theta_{\mathbf{p}'} - \theta_{\mathbf{k}'}) \\ & \phi_{\alpha}^*(\mathbf{k}) \phi_{\beta}^*(\mathbf{k}') \phi_{\gamma}(\mathbf{k}') \phi_{\delta}(\mathbf{k}) \\ & \phi_{\mu}^*(\mathbf{p}) \phi_{\nu}^*(\mathbf{p}') \phi_{\nu}(\mathbf{p}) \phi_{\mu}(\mathbf{p}') \end{aligned} \quad (40)$$

The internal sum over ν is self-averaging. While the most convincing way to show this is to compute its variance, and see that it is of order $1/\sqrt{g}$ times its average, this fact can be motivated in the following way: There is a sum over $g' \gg 1$ values of ν with a slowly varying energy denominator, which makes the sum over ν similar to a spectral average, which in RMT is the same as an average over the disorder ensemble. A more sophisticated argument is presented in Appendix A.

In RMT the wavefunction averages do not depend on the energy separations of the states, so the wavefunction average can be carried out separately. This average in the GOE for $\mu \neq \nu$ and generic momentum labels is

$$\begin{aligned} & \langle \phi_{\mu}^*(\mathbf{p}_1) \phi_{\nu}^*(\mathbf{p}_2) \phi_{\nu}(\mathbf{p}_3) \phi_{\mu}(\mathbf{p}_4) \rangle = \\ & \frac{\delta_{14} \delta_{23}}{g^2} - \frac{\delta_{13} \delta_{24}}{g^3} - \frac{\delta_{1,-2} \delta_{3,-4}}{g^3} \end{aligned} \quad (41)$$

The $1/g^2$ term is the “naive Wick contraction” of leading-order RMT, but the $1/g^3$ terms are necessary to maintain orthogonality between μ and ν . The final term would be missing in the GUE. Substituting the correct momentum labels for the particle-hole diagram we see that the wavefunction average is

$$\frac{\delta_{\mathbf{p}\mathbf{p}'}}{g^2} - \frac{1 + \delta_{\mathbf{p},-\mathbf{p}'}}{g^3} \quad (42)$$

Using the self-averaging shown in Appendix A, the first term of Eq.(42) forces $\mathbf{p} = \mathbf{p}'$ in Eq. (40). For large g , using

$$\sum_{\mathbf{p}} = g \int \frac{d\theta_{\mathbf{p}}}{2\pi} \quad (43)$$

we obtain a convolution of the two Fermi liquid functions

$$\sum_{\mathbf{p}} u(\theta_{\mathbf{k}} - \theta_{\mathbf{p}}) u(\theta_{\mathbf{p}} - \theta_{\mathbf{k}'}) = g(u_0^2 + \frac{1}{2} \sum_{m=1}^{\infty} u_m^2 \cos m(\theta - \theta')) \quad (44)$$

where we have reverted to the notation $\theta = \theta_{\mathbf{k}}$, $\theta' = \theta_{\mathbf{k}'}$. In the second term of Eq. (42), the $\delta_{\mathbf{p}, -\mathbf{p}'}$ turns out to be subleading, while the other allows independent sums over \mathbf{p} , \mathbf{p}' . This means that only u_0 contributes due to this term, which produces

$$\sum_{\mathbf{p}\mathbf{p}'} u(\theta_{\mathbf{k}} - \theta_{\mathbf{p}})u(\theta_{\mathbf{p}'} - \theta_{\mathbf{k}'}) = g^2 u_0^2 \quad (45)$$

We still need to do the energy sum, which we replace by an integral

$$\sum_{\varepsilon_\nu = -\Lambda}^0 \frac{1}{\Lambda + |\varepsilon_\nu|} \approx \int_0^\Lambda \frac{d\varepsilon}{\Delta} \frac{1}{\Lambda + \varepsilon} = \frac{\ln 2}{\Delta} \quad (46)$$

Feeding this into full expression for this contribution to the particle-hole diagram, we find it to be

$$\frac{g'}{g} \Delta \ln 2 \sum_{\mathbf{k}\mathbf{k}'} \left(\sum_{m=1}^{\infty} u_m^2 \cos m(\theta - \theta') \right) \phi_\alpha^*(\mathbf{k}) \phi_\beta^*(\mathbf{k}') \phi_\gamma(\mathbf{k}') \phi_\delta(\mathbf{k}) \quad (47)$$

Notice that the result is still of the Fermi liquid form. It is also seen that the contribution from u_0 cancels, about which we will say more below.

Now let us consider a contribution which is subleading in $1/g$ in the large- g limit.

$$\begin{aligned} & -g' \Delta^2 \sum_{\nu = -\Lambda}^0 \frac{1}{\Lambda + |\varepsilon_\nu|} \\ & \sum_{\mathbf{k}\mathbf{k}'} \sum_{\mathbf{p}\mathbf{p}'} u(\theta_{\mathbf{k}} - \theta_{\mathbf{p}})u(\theta_{\mathbf{p}'} - \theta_{\mathbf{k}'}) \\ & \phi_\alpha^*(\mathbf{p}) \phi_\beta^*(\mathbf{k}') \phi_\gamma(\mathbf{k}') \phi_\delta(\mathbf{k}) \\ & \phi_\mu^*(\mathbf{k}) \phi_\nu^*(\mathbf{p}') \phi_\nu(\mathbf{p}) \phi_\mu(\mathbf{p}') \end{aligned} \quad (48)$$

Note that the momentum labels of ϕ_α^* and ϕ_μ^* have been exchanged compared to Eq. (40) and there is a minus sign, both coming from the antisymmetrization of Eq. (31). Once again we ensemble average the internal μ , ν sum, the wavefunction part of which gives

$$\begin{aligned} & \langle \phi_\mu^*(\mathbf{k}) \phi_\nu^*(\mathbf{p}') \phi_\nu(\mathbf{p}) \phi_\mu(\mathbf{p}') \rangle = \\ & \frac{\delta_{\mathbf{k}\mathbf{p}'} \delta_{\mathbf{p}\mathbf{p}'}}{g^2} - \frac{\delta_{\mathbf{k}\mathbf{p}} + \delta_{\mathbf{k}, -\mathbf{p}'} \delta_{\mathbf{p}, -\mathbf{p}'}}{g^3} \end{aligned} \quad (49)$$

It is clear that there is an extra momentum restriction in each term compared to Eq. (42), which means that one can no longer sum freely over \mathbf{p} to get the factor of g in Eq. (44), or the factor of g^2 in Eq. (45). Therefore this contribution will be down by $1/g$ compared to that of Eq. (40). The general rule is that whenever a momentum label corresponding to an internal line in the diagram (here μ and ν) is forced to become equal to a momentum label corresponding to an external disorder label (here α, β, γ , or δ), the diagram is down by $1/g$, exactly as in the $1/N$ expansion.

Turning now to the Cooper diagrams, the internal lines are forced to have the same momentum labels as the external lines by the Fermi liquid vertex, therefore they do not make any leading contributions.

Finally, one can collect all the terms, and conclude that for $m \neq 0$

$$\frac{du_m}{d\xi} = -e^{-\xi} (\ln 2) u_m^2 \quad (50)$$

It must be emphasized that u_0 does not flow. The physical reason for this is that it commutes with the one-body ‘‘kinetic’’ part, and therefore does not suffer quantum fluctuations. The above equation can be written in a more physically transparent form by using a rescaled (for $m \neq 0$ only) variable

$$\tilde{u}_m = e^{-\xi} u_m \quad (51)$$

in terms of which the flow equation becomes

$$\frac{d\tilde{u}_m}{d\xi} = -\tilde{u}_m - (\ln 2) \tilde{u}_m^2 \equiv \beta(\tilde{u}_m) \quad (52)$$

where the last is a definition of the β -function. To understand the meaning of \tilde{u}_m we go back to Eq. (35), which expresses the variances of $V_{\alpha\beta\gamma\delta}$ in terms of u_m 's. We start with an ensemble of QD's with dimensionless conductance g . Suppose we wish to define a new ensemble with dimensionless conductance g' and Fermi liquid parameters u'_m , and demand that *all the statistical properties of the matrix elements, including the variances of Eq. (35), be the same*, we are led to

$$u'_0 = u_0 \quad (53)$$

$$\frac{u_m'^2}{g'^2} = \frac{u_m^2}{g^2} \Rightarrow u'_m = e^{-\xi} u_m \quad (54)$$

It is clear that the u'_m are exactly the \tilde{u}_m . From Eq. (52) it can be seen that positive initial values of \tilde{u}_m (which are equal to initial values of u_m inherited from the bulk) are driven to the fixed point at $\tilde{u}_m = 0$, as are negative initial values as long as $u_m(\xi = 0) \geq u_m^* = -1/\ln 2$. Thus, the Fermi liquid parameters are *irrelevant* for this range of starting values. Recall that setting all $u_m = 0$ for $m \neq 0$ results in the Universal Hamiltonian²⁰. Thus, the range $u_m \geq u_m^*$ is the basin of attraction of the Universal Hamiltonian. On the other hand, for $u_m(\xi = 0) \leq u_m^*$ results in a runaway flow towards large negative values of u_m , signalling a phase transition to a phase not perturbatively connected to the Universal Hamiltonian. Recall that the Pomeranchuk instability²⁷ of the clean spinless Fermi liquid happens for $u_m \leq -2$. The flow towards large negative values of u_m suggests that the system is undergoing some kind of Pomeranchuk instability. This notion turns out to be correct, and will be made precise in the next section. Note that there is a window $-2 \leq u_m \leq u_m^*$ in which the clean bulk system is stable while the system in a ballistic QD is unstable.

Let us summarize the results of the RG: (i) The RG equation is self-averaging for large g . (ii) The Fermi liquid form of the interactions is left unchanged to leading order by the RG flow. (iii) Each u_m flows separately, while u_0 does not flow. (iv) The flow equations show an instability for $u_m(\xi = 0) \leq u_m^* = -1/\ln 2$ in every Fermi

liquid channel, presumably towards a Pomeranchuk-like state. (v) The critical point shows a ‘‘correlation length’’ exponent $\nu = 1$, calculated from the slope of the β -function at the critical point.

$$\nu = \left(\frac{d\beta}{d\tilde{u}_m} \right)_{u_m^*} = 1 \quad (55)$$

B. Some Remarks on the Spinful Case

The case with spin is similar conceptually but somewhat more complicated technically than the spinless case. For a spin-rotationally-invariant Hamiltonian, the two-body interaction can be decomposed^{25,26} into a spin-singlet interaction function $u^{(s)}(\theta - \theta')$ and a spin-triplet interaction function $u^{(t)}(\theta - \theta')$. The projectors for the two two-body spin states are

$$\mathcal{P}^{(s)} = \frac{1 - \vec{\tau} \cdot \vec{\tau}'}{4} \quad (56)$$

$$\mathcal{P}^{(t)} = \frac{3 + \vec{\tau} \cdot \vec{\tau}'}{4} \quad (57)$$

where $\vec{\tau}$ and $\vec{\tau}'$ represent the Pauli spin operators for the two electrons (the numbers 1 and 3 in the numerators should be thought of as unit matrices in spin space). Writing the total interaction and comparing it to the Fermi liquid form (Eq. (12)) we find

$$u^{(s)}\mathcal{P}^{(s)} + u^{(t)}\mathcal{P}^{(t)} = \Phi + Z\vec{\tau} \cdot \vec{\tau}' \quad (58)$$

where all Fermi liquid labels and spin-matrix indices have been suppressed. This leads to the following relations

$$\Phi = \frac{u^{(s)} + 3u^{(t)}}{4} \quad (59)$$

$$Z = \frac{u^{(t)} - u^{(s)}}{4} \quad (60)$$

In order to carry out the RG, we define the interaction Hamiltonian as

$$H_I = \frac{1}{2} \sum_{ss', \alpha\beta\gamma\delta} V_{\alpha\beta\gamma\delta}^{ss'} c_{\alpha s}^\dagger c_{\beta s'}^\dagger c_{\gamma s'} c_{\delta s} \quad (61)$$

The one-loop scattering amplitude now reads as follows

$$\begin{aligned} \Gamma_{\alpha\beta\gamma\delta}^{ss'} &= V_{\alpha\beta\gamma\delta}^{ss'} \\ &+ \sum_{\mu\nu} \frac{N_F(\nu) - N_F(\mu)}{\varepsilon_\mu - \varepsilon_\nu} \left(V_{\alpha\mu\nu}^{ss'} V_{\beta\nu\delta}^{s's} - V_{\alpha\mu\nu}^{ss} V_{\beta\nu\delta}^{s's'} \right. \\ &\quad \left. - V_{\beta\nu\mu}^{s's'} V_{\alpha\mu\nu}^{ss'} - \sum_{s_1} V_{\alpha\mu\nu}^{ss_1} V_{\beta\nu\mu}^{s'_1 s'} \right) \\ &- \sum_{\mu\nu} \frac{1 - N_F(\mu) - N_F(\nu)}{\varepsilon_\mu + \varepsilon_\nu} V_{\alpha\beta\mu\nu}^{ss'} V_{\nu\mu\gamma\delta}^{ss'} \end{aligned} \quad (62)$$

In order to separate $V_{\alpha\beta\gamma\delta}^{ss'}$ into its singlet and triplet components, we need two facts: (i) The singlet channel

is characterized by antisymmetry in spin, and therefore symmetry in the orbital labels of the incoming (and separately, the outgoing) particles. The triplet channel is exactly the reverse. (ii) If $s = s'$ then the interaction is forced to be in the triplet channel. However, if $s \neq s'$ the interaction is a superposition of the singlet and triplet channels.

On the above basis we identify the singlet and triplet channel interactions as

$$V_{\alpha\beta\gamma\delta}^{(s)} = \frac{1}{4} \left(V_{\alpha\beta\gamma\delta}^{\uparrow\downarrow} + V_{\beta\alpha\gamma\delta}^{\uparrow\downarrow} + V_{\alpha\beta\delta\gamma}^{\uparrow\downarrow} + V_{\beta\alpha\delta\gamma}^{\uparrow\downarrow} \right) \quad (63)$$

$$V_{\alpha\beta\gamma\delta}^{(t)} = \frac{1}{4} \left(V_{\alpha\beta\gamma\delta}^{\uparrow\downarrow} - V_{\beta\alpha\gamma\delta}^{\uparrow\downarrow} - V_{\alpha\beta\delta\gamma}^{\uparrow\downarrow} + V_{\beta\alpha\delta\gamma}^{\uparrow\downarrow} \right) = V_{\alpha\beta\gamma\delta}^{\uparrow\uparrow} \quad (64)$$

and the inverse relations

$$V_{\alpha\beta\gamma\delta}^{\uparrow\uparrow} = V_{\alpha\beta\gamma\delta}^{(t)} \quad (65)$$

$$V_{\alpha\beta\gamma\delta}^{\uparrow\downarrow} = V_{\alpha\beta\gamma\delta}^{(s)} + V_{\alpha\beta\gamma\delta}^{(t)} \quad (66)$$

In order to carry out the wavefunction averages one expresses these matrix elements as

$$\begin{aligned} V_{\alpha\beta\gamma\delta}^{(s)} &= \frac{\Delta}{4} \sum_{\mathbf{k}\mathbf{k}'} u^{(s)}(\theta - \theta') \left[\phi_\alpha^*(\mathbf{k})\phi_\beta^*(\mathbf{k}') + \phi_\alpha^*(\mathbf{k}')\phi_\beta^*(\mathbf{k}) \right] \\ &\quad \times [\phi_\gamma(\mathbf{k}')\phi_\delta(\mathbf{k}) + \phi_\gamma(\mathbf{k})\phi_\delta(\mathbf{k}')] \end{aligned} \quad (67)$$

$$\begin{aligned} V_{\alpha\beta\gamma\delta}^{(t)} &= \frac{\Delta}{4} \sum_{\mathbf{k}\mathbf{k}'} u^{(t)}(\theta - \theta') \left[\phi_\alpha^*(\mathbf{k})\phi_\beta^*(\mathbf{k}') - \phi_\alpha^*(\mathbf{k}')\phi_\beta^*(\mathbf{k}) \right] \\ &\quad \times [\phi_\gamma(\mathbf{k}')\phi_\delta(\mathbf{k}) - \phi_\gamma(\mathbf{k})\phi_\delta(\mathbf{k}')] \end{aligned} \quad (68)$$

Now it is straightforward to find the RG flows of the singlet and triplet Landau interaction functions. A non-trivial check is provided by the fact that there are two expressions for the triplet interaction, and their flows should be identical. These flows can be written in terms of the rescaled Landau parameters $\tilde{\Phi}_m = e^{-\xi}\Phi_m$ and $\tilde{Z}_m = e^{-\xi}Z_m$, and one obtains to leading order in $1/g$

$$\frac{d\tilde{\Phi}_m}{d\xi} = -\tilde{\Phi}_m - (2\ln 2)\tilde{\Phi}_m^2 \quad (69)$$

$$\frac{d\tilde{Z}_m}{d\xi} = -\tilde{Z}_m - (2\ln 2)\tilde{Z}_m^2 \quad (70)$$

Clearly, the charge and spin channels flow independently, and there is an instability at $-1/(2\ln 2) = -0.7213\dots$ in each channel. Recall that in the clean Fermi liquid the Pomeranchuk instability occurred at -1 in our normalization. Thus, there is a substantial window where the clean system in the bulk is stable, but the ballistic system is unstable.

C. Unanswered Questions in the RG

While the RG makes it plausible that there is indeed a transition out of the phase controlled by the Universal Hamiltonian, it leaves two important questions unanswered. Recall that we have used a one-loop calculation of the scattering amplitude to define the RG flow. This

is usually sufficient when the dimensionless couplings u_m are much smaller than unity. However, the critical point occurs when u_m is of order unity. Can we trust the one-loop calculation at this point? In other words, suppose there were higher-order diagrams in the scattering amplitude to leading order in $1/g$. This would have generated cubic and higher-order terms in the RG flow. For a sufficiently large value of the cubic term, the critical point identified in the previous subsections can disappear. In that case it would have been an artifact based on an invalid approximation. Secondly, even if we accept the phase transition as genuine, the RG gives us no way of calculating physical quantities in the strong-coupling phase. Both of these questions are answered in the next section, where we show that the one-loop flow is exact in the large- g limit, and that there is a controlled way of calculating all the properties of the strong-coupling phase in a large- N approximation.

IV. LARGE- N THEORY OF THE MESOSCOPIC POMERANCHUK REGIMES

As the name suggests, large- N theories typically involve interactions between N species of objects. The largeness of N renders fluctuations (thermal or quantum) small, and enables one to make approximations which are not perturbative in the coupling constant, but are controlled by the additional small parameter $1/N$. Large- N approximations have found many uses in condensed matter physics, but usually the value of N which characterizes the real model is quite small (2 or 3). We will find below that ballistic mesoscopic structures offer a realization of large- N theory where $N = g$. The g momentum states act as g “species” of fermions. Thus, one can make N as large as one wants modulo technological challenges. In fact, standard Fermi Liquid theory in a clean bulk system can also be formulated in this way²⁸.

There are two primary manifestations of the large- N nature of a theory: (i) The four-point scattering amplitude is dominated by iterated particle-hole diagrams. (ii) The effective action is dominated by its saddle-point.

In this section we will demonstrate each of these manifestations of large- N theory, and end by solving the strong-coupling theory in a saddle-point approximation.

A. Diagrammatic Large- N and the Exactness of One-Loop RG in the Large- g Limit

To put the issue in context, let us consider the Gross-Neveu model⁴⁸ which is one of the simplest fermionic large- N theories. This theory has N identical massless relativistic fermions interacting by an attractive short-range interaction. The Lagrangian density is

$$\mathcal{L} = \sum_i \bar{\psi}_i \not{\partial} \psi_i - \frac{\lambda}{N} \left(\sum_i \bar{\psi}_i \psi_i \right)^2 \quad (71)$$

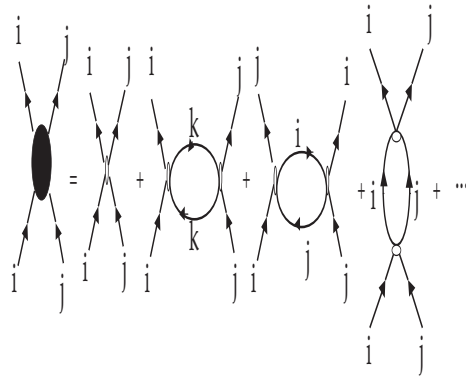


FIG. 2. The first few Feynman diagrams in the four-point scattering amplitude for the Gross-Neveu theory.

Note that the propagator conserves the internal index, as does the interaction term.

Figure 2 shows the first few diagrams in the expression for the four-point scattering amplitude (for particles of species i and j to scatter) in the Gross-Neveu theory. The “bare” vertex comes with a factor λ/N . The one-loop diagrams all share a factor λ^2/N^2 from the two vertices. The first one-loop diagram has a free internal summation over the index k over N values, with the contribution being identical for each value of k . Thus, this one-loop diagram acquires a compensating factor of N which makes its contribution of order λ^2/N , the *same order in $1/N$ as the bare vertex*. However, the other one-loop diagrams have no such free internal summation and their contribution is indeed of order $1/N^2$. Therefore, to leading order in $1/N$, one should keep only diagrams which have a free internal summation for every vertex, that is, iterates of the leading one-loop diagram, which are called bubble graphs. *For later use remember that in the diagrams that survive (do not survive), the indices i and j of the incoming particles do not (do) enter the loops*. Let us assume that the momentum integral up to the cutoff Λ for one bubble gives a factor $\Pi(\Lambda, q_{ext})$, where q_{ext} is the external momentum transfer at which the scattering amplitude is evaluated. To leading order in large- N the full expression for the scattering amplitude is

$$\Gamma_{ij}(q_{ext}) = \frac{1}{N} \frac{\lambda}{1 + \lambda \Pi(\Lambda, q_{ext})} \quad (72)$$

Once one has the full expression for the scattering amplitude (to leading order in $1/N$) one can ask for the RG flow of the “bare” vertex as the cutoff is reduced by demanding that the physical scattering amplitude Γ remain insensitive to the cutoff. One then finds

$$\frac{d\Gamma_{ij}(q_{ext})}{d\xi} = 0 \Rightarrow \frac{d\lambda}{d\xi} = \lambda^2 \frac{d\Pi(\Lambda, q_{ext})}{d\xi} \quad (73)$$

where $\xi = \ln(\Lambda_0/\Lambda)$ is the flow parameter of the RG. This equation shows that *the one-loop RG flow is the exact answer to leading order in a large- N theory*. All higher-order corrections must therefore be subleading in $1/N$.

Let us now turn to our theory, in which the role of the internal index is played by the momentum patch label \mathbf{k} , which can take on g values. The role of the coupling constant λ in our theory is played by $E_T u(\theta - \theta')$. From the definition of the matrix elements in Eq. (31) we see that interactions occur in the Hamiltonian as $E_T u(\theta - \theta')/g$ in analogy with the λ/N in the Gross-Neveu Lagrangian. Let us remark in this context that the most natural way to take the large- g limit is to keep E_T fixed and decrease Δ .

The major departure from the Gross-Neveu theory is that in our theory the propagator does not conserve the label \mathbf{k} . The contributions of the leading and subleading one-loop diagrams were presented in Eqs. (40,48) respectively. The crucial fact which allows us to show the large- N nature of this theory is the self-averaging of the internal summations, which follows from the arguments of the previous section (and Appendix A). This self-averaging means that the internal wavefunction products can be replaced by their ensemble averages, which by Eq. (41) makes the internal propagators effectively momentum-conserving. Now the analogy to the Gross-Neveu theory is complete.

From this analogy we learn that the one-loop RG flow computed by two of us⁹ is indeed the exact answer in the large- g limit, and that the phase transition it indicates is real. However, this analogy is even more fruitful in providing a way to compute physical quantities in the strong-coupling phase¹⁰, to a description of which we now turn.

B. The Effective Theory of the Strong-Coupling Phase

The strong-coupling phase occurs for $u_m < u_m^*$ for any m . We will consider the simplest situation, when just one angular momentum channel undergoes an instability. This is not an artificial restriction for two reasons: Firstly, as seen in the RG treatment, the instabilities in different channels are independent. Secondly, it is highly unlikely that more than one Landau parameter is close to an instability in a generic system. Furthermore, we will restrict our attention to charge-channel instabilities in the spinful case, in which the spin index is a passive spectator. This may turn out to be the experimentally relevant type of instability; looking at the Landau parameters⁴² for the clean bulk 2DEG at $r_s = 5$ (Eq. (21)) we see that the $m = 2$ charge channel is the one closest to an instability. Instabilities in the spin channel are extremely interesting, but in treating them one must necessarily also account for the exchange coupling J . The resulting theory thus depends on two parameters (Z_m, J), and will be investigated in detail in a future publication.

Thus, our model Landau interaction function for this section is

$$u_m \cos m(\theta - \theta') \quad (74)$$

with no sum over m . All the thermodynamic properties of the system can be obtained from the partition function Z , which can be converted into a path integral in imaginary time by performing the usual time-slicing according to

$$Z = \text{Tr} \left(e^{-\beta H} \right) = \text{Tr} \lim_{\mathcal{N} \rightarrow \infty} \prod_i^{\mathcal{N}} e^{-\beta H/\mathcal{N}} \quad (75)$$

where $\beta = 1/T$ is the inverse temperature. One then inserts a complete set of fermionic coherent states between each factor of $e^{-\beta H/\mathcal{N}}$, and writes the matrix elements in terms of the coherent state labels. In the process, the fermionic operators c, c^\dagger get replaced by Grassmann numbers, which we will represent by $\psi, \bar{\psi}$. The partition function can now be written as

$$Z = \int D\psi D\bar{\psi} e^{-S} \quad (76)$$

where

$$S = \int_{-\beta/2}^{\beta/2} dt \left(\sum_{\alpha} \bar{\psi}_{\alpha}(t) \left(\frac{\partial}{\partial t} + \varepsilon_{\alpha} \right) \psi_{\alpha}(t) - \frac{|u_m| \Delta}{2} \sum_{\mathbf{k}, \mathbf{k}'} \cos m(\theta - \theta') n_{\mathbf{k}}(t) n_{\mathbf{k}'}(t) \right). \quad (77)$$

Here $n_{\mathbf{k}}(t) = \bar{\psi}_{\mathbf{k}}(t) \psi_{\mathbf{k}}(t)$ and we have made explicit the fact that $u_m < 0$. We factorize the interaction term in one time slice (of thickness $\delta t = \beta/\mathcal{N}$):

$$\begin{aligned} & \exp \left[\delta t \frac{\Delta}{2} \sum_{\mathbf{k}, \mathbf{k}'} |u_m| \cos(m\theta - m\theta') n_{\mathbf{k}} n_{\mathbf{k}'} \right] = \\ & \int d\boldsymbol{\sigma} \exp -\delta t \Delta \left[g^2 \frac{|\boldsymbol{\sigma}|^2}{2|u_m|} + g \sum_{\mathbf{k}} n_{\mathbf{k}} (\sigma_1 \cos m\theta + \sigma_2 \sin m\theta) \right] \\ & = \int d\boldsymbol{\sigma} \exp \left[-g^2 \delta t \Delta \frac{|\boldsymbol{\sigma}|^2}{2|u_m|} - g \delta t \Delta \sum_{\alpha\beta} \bar{\psi}_{\alpha} \boldsymbol{\sigma} \cdot \mathbf{M}_{\alpha\beta} \psi_{\beta} \right] \end{aligned}$$

where $\boldsymbol{\sigma} = (\sigma^1, \sigma^2)$ has two components, as does \mathbf{M} : $(M^1, M^2)_{\alpha\beta} = \sum_{\mathbf{k}} \phi_{\alpha}^*(\mathbf{k}) \phi_{\beta}(\mathbf{k}) (\cos m\theta, \sin m\theta)$. Note that this factorization with a real action for $\boldsymbol{\sigma}$ can be carried out only for $u_m < 0$, which is indeed the case here. The factors of g are chosen for later convenience.

The fermionic action is now quadratic, and the fermions can be integrated out to obtain an effective action for $\boldsymbol{\sigma}$

$$S_{eff} = -\text{Tr} \ln [(i\omega - \varepsilon_{\alpha}) \mathbf{I} - g \Delta \boldsymbol{\sigma} \cdot \mathbf{M}] + g^2 \Delta \int dt \frac{|\boldsymbol{\sigma}|^2}{2|u_m|} \quad (78)$$

where I is the unit matrix and $\boldsymbol{\sigma}$ is now a function of imaginary time t .

To make further progress we expand S_{eff} in powers of $\boldsymbol{\sigma}$, which can be expressed graphically by the set of ‘‘ring diagrams’’ shown in Fig. 3.

Evaluating the diagram with two external $\boldsymbol{\sigma}$ legs, we find the following quadratic contribution from the $\text{Tr} \ln$ in the static limit (when fluctuations of $\boldsymbol{\sigma}$ in imaginary time are ignored):

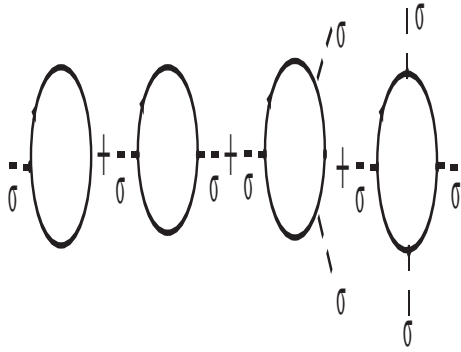


FIG. 3. The Feynman diagrams in the graphical expansion of the Trace Log. Each diagram has one fermion loop with different numbers of external σ legs.

$$g^2 \Delta^2 \int dt \sum_{\alpha\beta} \frac{N_F(\beta) - N_F(\alpha)}{\varepsilon_\alpha - \varepsilon_\beta} \sum_{\mathbf{k}, \mathbf{k}'} \phi_\alpha^*(\mathbf{k}) \phi_\beta(\mathbf{k}) \phi_\beta^*(\mathbf{k}') \phi_\alpha(\mathbf{k}') (\sigma_1 \cos m\theta + \sigma_2 \sin m\theta)(\sigma_1 \cos m\theta' + \sigma_2 \sin m\theta') \quad (79)$$

where $N_F(\alpha)$ is the Fermi occupation of the single-particle state α .

This quantity can be recognized as the one that appears in the internal summation of the leading large- N one loop bubble, Eq. (40). As mentioned before (and shown in Appendix A) this quantity is self-averaging; its disorder-average dominates its fluctuations by g . We carry out this self-averaging using RMT to obtain the average quadratic part of the action for static σ

$$\bar{S}_0 = g^2 \int dt \frac{|\sigma|^2 \Delta}{2} \left[\frac{1}{|u_m|} - \ln 2 \right] \quad (80)$$

where the bar represents the fact that we are considering only the (self-) disorder-averaged part of S_0 , and the $\ln 2 = 1/|u_m^*|$ arises from the summation over energies in Eq. (79). For the spinful case this number would be twice as large. It is clear that for $|u_m| < |u_m^*|$, $\sigma = 0$ is a stable solution, while σ will break symmetry for $|u_m| > |u_m^*|$. In both cases let

$$r = \frac{1}{|u_m|} - \frac{1}{|u_m^*|} \quad (81)$$

denote the distance from criticality.

Will this symmetry-breaking, present in the “bare” theory, survive fluctuations? The answer to this hinges on the fact that a factor g^2 appears at all higher loops, i.e., in front of the entire self-averaged action for static σ . The 4th-order term suffices to clarify the issue. The generic 4th-order term is shown in Figure 4, and is represented by the following expression (all factors except for g have been suppressed):

$$g^4 \sigma^4 \sum_{\alpha\beta\gamma\delta} \frac{M_{\alpha\beta} M_{\beta\gamma} M_{\gamma\delta} M_{\delta\alpha}}{\varepsilon^3} \quad (82)$$

where ε is a generic energy denominator.

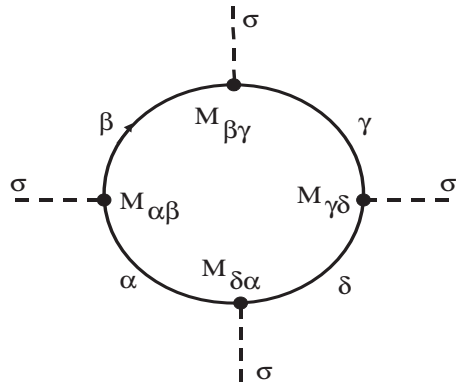


FIG. 4. The Feynman diagram corresponding to the fourth-order term in the effective action.

We now replace the product of wavefunction sitting inside the M 's by their averages, giving the usual arguments about self-averaging. Just as the average of four ϕ 's had many terms corresponding to different contractions of indices (Eqn. (34)), there are many terms here as well. In the leading contribution, the ϕ_β from $M_{\alpha\beta}$ is contracted with the ϕ_β^* from $M_{\beta\gamma}$ and so on around the loop. This forces the same \mathbf{k} index to flow around the loop, generating the factor $\sum_{\mathbf{k}} 1/g^4 = 1/g^3$. There are 4 energy summations (going up to $g\Delta$) and three factors of energy in the denominator (each typically of order $g\Delta$), leading to an extra factor of g . The overall result is therefore of order $g^2\sigma^4$.

It can be shown along very similar lines that the factor of g^2 can be extracted from the entire self-averaged effective action in the static limit. Thus g^2 plays the role of $1/\hbar$ (or the inverse temperature), and controls the size of fluctuations around the saddle-point. This is what renders the large- N approximation realistic for ballistic dots with large dimensionless conductance.

Armed with the factor of g^2 multiplying the entire static self-averaged effective action, one can see that the saddle-point approximation becomes exact in the large- g limit, and therefore our conclusion that symmetry-breaking takes place for $|u_m| > |u_m^*|$ is in fact correct in this limit.

To see what the order parameter corresponds to, recall that in terms of the original fermions $\langle(\sigma_1, \sigma_2)\rangle = \sum_{\mathbf{k}} \langle n_{\mathbf{k}} \rangle (\cos m\theta, \sin m\theta)$, where $\langle \rangle$ denotes a quantum-mechanical (but not disorder-ensemble) averaging. This shows that some values of \mathbf{k} are preferentially occupied compared to others. Therefore this can be identified as the mesoscopic, disordered, version of the Pomeranchuk shape transition of the Fermi surface^{27,26}. There has been a revival of interest in the bulk transition recently^{43,44}. Due to the disorder, \mathbf{k} is not a good quantum number, and $n_{\mathbf{k}}$ will suffer quantum fluctuations, unlike the clean bulk case. The quantum-mechanical average $\langle n_{\mathbf{k}} \rangle$ is similarly not restricted to be 0 or 1. The Fermi “surface” will not be sharp, but will be smeared out by the disorder. However, the angular average corresponding to σ still provides an unambiguous measure of symmetry-breaking.

C. The Connection of Large- N to the Hartree Approximation

The static large- N saddle-point solution is the same as standard Hartree mean field theory (the Fock term is down by $1/g$ because of the form of the Fermi liquid interaction). This can be seen very easily by noting that the saddle point satisfies the self-consistency condition

$$\frac{d}{d\boldsymbol{\sigma}} \left(-Tr \ln [(i\omega - \varepsilon_\alpha)\mathbf{I} - g\Delta\boldsymbol{\sigma} \cdot \mathbf{M}] + g^2\Delta \int dt \frac{|\boldsymbol{\sigma}|^2}{2|u_m|} \right) = 0 \quad (83)$$

The above equation in fact minimizes the expression for β times the free energy, or just the ground state energy as $T \rightarrow 0$. Note that it has two parts, one from the fermionic $Tr \ln$ and one from the $\boldsymbol{\sigma}$ field energy, $\frac{|\boldsymbol{\sigma}|^2\Delta}{2|u_m|}$.

Using the Feynman-Hellman theorem, which equates the $\boldsymbol{\sigma}$ derivative of the expectation value of the fermion hamiltonian to the expectation value of the derivative of the fermion hamiltonian, we have

$$T \frac{d}{d\boldsymbol{\sigma}} \left(-Tr \ln [(i\omega - \varepsilon_\alpha)\mathbf{I} - g\Delta\boldsymbol{\sigma} \cdot \mathbf{M}] \right) = g\Delta \langle SD(\boldsymbol{\sigma}) | \sum_{\mathbf{k}} n_{\mathbf{k}} (\cos m\theta\hat{i} + \sin m\theta\hat{j}) | SD(\boldsymbol{\sigma}) \rangle \quad (84)$$

where we have introduced the Slater Determinantal state $|SD(\boldsymbol{\sigma})\rangle$, which is obtained by diagonalizing the Hamiltonian with a static $\boldsymbol{\sigma}$, and filling up the lowest $g/2$ levels. This leads to the self-consistency condition

$$u_m \langle SD(\boldsymbol{\sigma}) | \sum_{\mathbf{k}} n_{\mathbf{k}} (\cos m\theta\hat{i} + \sin m\theta\hat{j}) | SD(\boldsymbol{\sigma}) \rangle = g\boldsymbol{\sigma} \quad (85)$$

This is exactly the condition one would get by decoupling the interaction in a Hartree approximation, which indicates that at the saddle-point level, the large- N theory is the same as the Hartree approximation. However, the large- N nature of the theory allows one to justify the saddle-point, and to systematically calculate corrections to it.

V. PHASE DIAGRAM AND PHYSICAL SIGNATURES

We now turn to qualitative and quantitative consequences of the large- g solution. Our discussion will use the language of phase transitions - collective variables becoming gapless and order parameters turning on at criticality - but there will be inevitable modifications due the fact that we are primarily interested in a mesoscopic system with discrete energy levels.

Let us begin by reiterating that a genuine phase transition occurs only in the limit $g \rightarrow \infty$. This is a mathematical idealization that allows one to study and classify dots, but is inaccessible in practice because $\Delta \simeq 1/L^2$, $E_T \simeq$

$1/L$, and their ratio $g \simeq L$. Thus the limit $g \rightarrow \infty$, corresponds $L \rightarrow \infty$, i.e., a dot of infinite size. In such a system $E_T \rightarrow 0$ and everything we discuss (states sensitive to boundary conditions and a phase transition that precedes that of the clean bulk system) occurs within an energy window of zero thickness and is thus invisible. This is to be expected because in this limit we are really describing an infinite ballistic system. [†]

We shall refer to the transition that occurs within E_T in the $g \rightarrow \infty$ limit as the mesoscopic Pomeranchuk transition. With the above words of explanation, the reader should not have any trouble reconciling the juxtaposition of the words mesoscopic and phase transition in one phrase.

While the $g \rightarrow \infty$ quantum dot is not directly accessible, we are interested in it because several nontrivial features of the phase transition it undergoes manifest themselves even for $1/g > 0$. This result is based on recent investigations into quantum phase transitions, which show that while the $T = 0$ transition (as a function of some coupling) occurs at an isolated point that is also physically inaccessible, it controls the physical behavior in a fan-shaped quantum critical regime³¹ in the temperature-coupling constant plane. In our problem $1/g$ plays the role of T since g^2 multiplies the action. The situation is depicted in Figure 4. The dotted lines bounding the quantum critical regime indicate the sharp crossover which replaces the transition. There are however some differences from the usual quantum critical descriptions because g not only appears outside the action and plays the role of inverse temperature, but also appears within S_{eff} via subleading, disorder-realization-specific terms which are especially important in the strong-coupling phase.

In this section we will explore the three regimes: weak-coupling, strong-coupling, and quantum-critical as well as crossovers between them. The physics of the weak-coupling regime is controlled by the Universal Hamiltonian. However, we will point out that even in a system belonging to this regime one can access the physics of the quantum-critical regime by making a finite frequency measurement. Thus even dots in this region can be used to confirm the existence of the phase transition we have found at u^* .

We first turn to the strong-coupling and quantum-critical regimes which are new to our work.

[†]This idealization was also implied in RG analysis when it gave a zero of the β function at u^* . In order to get singular behavior out of a zero of a β -function, we need to be able to carry out the RG transformation an indefinite number of times. This means E_T must contain an infinite number of states. In a real dot the flow ends when we come to within Δ of the Fermi surface. Thus the critical state with $r = 0$ is characterized by the fact that $\boldsymbol{\sigma}$ has gap of order Δ as compared to the generic value of $g\Delta$.

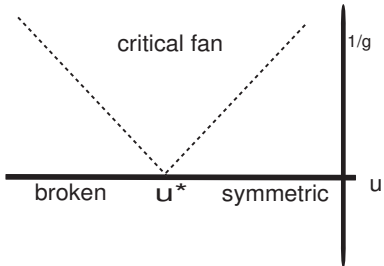


FIG. 5. The generic phase diagram for a second-order quantum phase transition. The horizontal axis represents the coupling constant which can be tuned to take one across the transition. The vertical axis is usually the temperature in bulk quantum systems, but is $1/g$ here, since in our system one of the roles played by g is that of the inverse temperature.

A. The Strong-Coupling Regime

As shown by Eq. (80) σ acquires a nonzero expectation value if $u_m < u_m^*$ or $r < 0$. Since σ can be thought of as a two-dimensional vector order parameter, and the self-averaging part of S_{eff} has rotational symmetry, one expects a Mexican Hat (a circle of exactly degenerate minima $|\sigma| = \sigma_0$). For $g = \infty$ the system can still break symmetry and pick a particular value of σ , since there are no kinetic term for σ in that limit (see Eq. (87) below). However, for $1/g \neq 0$ one may expect that σ will delocalize immediately around the Mexican Hat, restoring symmetry, since $1/g^2$ plays the role of T or \hbar (depending on how one wants to interpret the path integral). In other words one expects the zero-dimensional analog of the Mermin-Wagner theorem⁴⁹. In terms of the parameterization of σ in cylindrical coordinates

$$\sigma = (\sigma, \chi) \quad (86)$$

we expect the σ variable to uniformly populate all values of the angle χ .

This does not actually happen, thanks to disorder-realization-specific terms in S_{eff} , which are subleading in $1/g$ to the terms considered so far and explicitly break rotational symmetry in σ space. There are many sources for such $1/g$ terms. The coefficient of the quadratic term coming from the $Tr \ln$, which has a leading average part which produces the $\ln 2$, also has sample-to-sample fluctuations which are down by $1/g$ (as shown in Appendix A). In fact, a term *first-order* in σ is also present for a system undergoing an instability in an even angular momentum channel m . These subleading terms render the valley of the Mexican Hat nondegenerate in the case of even m , and leave behind a two-fold degeneracy in the case of m odd.

Will these sample specific terms localize σ in the angular direction? To resolve this issue we need to understand the low-energy dynamics of σ . To this end we compute

the quadratic part of the effective action for slow fluctuations of σ . We find

$$\bar{S}_0 = g^2 \int dt \frac{|\dot{\sigma}|^2 \Delta}{2} \left[\frac{1}{|u_m|} - \frac{1}{|u_m^*|} \right] + g \int \frac{d\omega}{2\pi} |\sigma(\omega)|^2 f(\omega) \quad (87)$$

where the bar represents the fact that we are considering only the (self-) disorder-averaged part of S_0 . The frequency dependent function $f(\omega)$ is

$$f(\omega) = \frac{1}{4} \left(2\omega \tan^{-1} \frac{\omega}{\Delta} + 2\omega \tan^{-1} \frac{\omega}{\Lambda} - 4\omega \tan^{-1} \frac{2\omega}{\Lambda} + \Lambda \ln \left[\frac{(4\omega^2 + \Lambda^2)}{(\omega^2 + \Lambda^2)} \right] - \Delta \ln \left[1 + \frac{\omega^2}{\Delta^2} \right] \right) \quad (88)$$

Let us note that

$$f(\omega) = \omega^2/4\Delta \quad \omega \ll \Delta \quad (89)$$

$$= \pi|\omega|/4 \quad \Delta \ll \omega \ll E_T \quad (90)$$

Thus we expect Hamiltonian dynamics at very low energies, with a non-universal sample specific dependence on the lower cutoff Δ . At high energies we have overdamped dynamics, representing the effect of Landau damping on the σ variable. This latter behavior is universal and self-averaging.[‡]

At very low energies described by hamiltonian dynamics Eqs. (89,) the momentum conjugate to σ is

$$\mathbf{p}\sigma = g\dot{\sigma}/2\Delta. \quad (91)$$

Only the angular dynamics is important in the symmetry-broken phase since the radial fluctuations of σ are suppressed by the Mexican Hat potential of order $g^2\Delta$. The Hamiltonian for small oscillations around the global minimum of the explicit symmetry-broken effective action looks like

$$H_{osc} = \Delta \frac{\hat{L}^2}{g} + g\Delta V(\chi) \quad (92)$$

where we have denoted the angular part of the canonical momentum as \hat{L} . The spread of the ground state wave function (of this oscillator) can be estimated as $\delta\chi \simeq 1/\sqrt{g}$. Thus at large g the support of σ is localized to the minimum of the potential energy term. Our analysis is internally consistent: The form of $f(\omega)$ we used to

[‡]The reader might ask what permits us to keep some terms which are $1/g$ down compared to the self-averaged static part of S_{eff} , and discard others. The answer is that we keep only the lowest order terms of every type. Thus, the realization-specific terms which break the rotational symmetry of the self-averaged part of S_{eff} are kept, while $1/g$ corrections to the self-averaged part are discarded. Similarly, though the kinetic term of Eq. (87) is order $1/g$ down compared to the self-averaged part, it must be kept since this is the lowest order dynamics.

obtain oscillator description (Eqn. (89)) is valid out to $\omega \simeq \Delta$, the oscillator ground state energy.³

Thus symmetry-breaking will occur in the strong-coupling regime for large enough g when disorder-realization-specific terms are included. The result is a consequence of spontaneous symmetry-breaking (requiring strong interactions) and explicit symmetry-breaking (from disorder).

These considerations apply uniformly for m even and odd. However, there are significant differences in other features and we will treat them separately.

1. The Case of m Even

Let us see how to find the effective potential with the realization-specific corrections more explicitly. We need to find the ‘‘potential landscape’’ of σ , which we define for t -independent σ as

$$V_{eff}(\sigma) = g^2 \Delta \frac{\sigma^2}{2|u_m|} - \frac{1}{\beta} Tr \ln[(i\omega - \varepsilon_\alpha) \delta_{\alpha\beta} - g \Delta \sigma \cdot \mathbf{M}_{\alpha\beta}] \quad (93)$$

where $\beta = 1/T$ is the inverse temperature not to be confused with the label for noninteracting disorder eigenstates. We thus need to map out the $Tr \ln$ for time-independent σ . In the limit of zero temperature, the quantity $Tr \ln(i\omega - H_{F,\sigma})/\beta$ is just $-\mathcal{E}_F(\sigma)$, where the fermionic Hamiltonian is

$$H_{F,\sigma} = \sum_\alpha \varepsilon_\alpha c_\alpha^\dagger c_\alpha - g \Delta \sigma \cdot \sum_{\alpha\beta} \mathbf{M}_{\alpha\beta} c_\alpha^\dagger c_\beta \quad (94)$$

and $\mathcal{E}_F(\sigma)$ is its ground state energy, obtained by diagonalizing the hamiltonian $H_{F,\sigma}$ and filling up the lowest states with the requisite number of fermions. Let us note that for large g , since fluctuations in σ are small, we can approximate the *total energy of the interacting system with N particles* \mathcal{E}_N as the minimum of the effective potential of Eq. (93),

$$\mathcal{E}_N = Min_\sigma \left(\mathcal{E}_F(\sigma) + \frac{g^2 \Delta \sigma^2}{2|u_m|} \right) \quad (95)$$

where Min_σ indicates that the argument should be minimized over all σ . Note that the value of σ at the minimum depends on the realization as well as the number of particles N .

For small σ we can find \mathcal{E}_F by standard perturbation theory. To first order we find the following energy correction

$$\mathcal{E}_F^{(1)}(\sigma, \chi) = -g \Delta \sigma \cdot \sum_{\alpha occ} \mathbf{M}_{\alpha\alpha} \quad (96)$$

$$= -g \Delta \sigma \sum_{\mathbf{k}, \alpha occ} \phi_\alpha^*(\mathbf{k}) \phi_\alpha(\mathbf{k}) \cos(m\theta - \chi) \quad (97)$$

where the sum is over occupied states only, and σ , χ are the magnitude and angle of σ respectively. From the fact that $\phi_\alpha^*(\mathbf{k}) = \phi_\alpha(-\mathbf{k})$ it follows that

$$\mathbf{M}_{\alpha\beta} = (-1)^m \mathbf{M}_{\beta\alpha}^* \quad (98)$$

a specific instance of which is

$$\mathbf{M}_{\alpha\alpha} = (-1)^m \mathbf{M}_{\alpha\alpha} \quad (99)$$

This in turn shows that $\mathbf{M}_{\alpha\alpha}$ must vanish for odd m . However, for even m there is no reason for this to vanish for a particular disorder realization (though its disorder-average does vanish). One can also see that this term produces a dependence on the angle χ of σ , which breaks the degeneracy of states in the Mexican Hat. To get an idea of the magnitude of this realization-dependent term, we square it and average over disorder. It is easy to verify that the disorder ensemble average (denoted by $\langle\langle \rangle\rangle$) is given by

$$\langle\langle (\mathcal{E}_F^{(1)})^2 \rangle\rangle \simeq g^2 \Delta^2 \quad (100)$$

meaning that the typical size of this correction is of order g , one power of g down from the self-averaging part of \mathcal{E} .

One can also analytically get the statistical correlations in the shape of the first-order contribution to the potential by computing

$$\langle\langle \mathcal{E}_F^{(1)}(\chi_1) \mathcal{E}_F^{(1)}(\chi_2) \rangle\rangle \simeq g^2 \Delta^2 \cos(\chi_1 - \chi_2) \quad (101)$$

The picture we get for even m is then the following: Each order in perturbation theory contributes a fairly smooth (on average) realization-dependent term which depends on χ , thus breaking the symmetry of the $g = \infty$ Mexican Hat. If the system is not too deep in the strong-coupling phase we can expect that only a few orders of perturbation theory contribute, and that the angle-dependent potential in the Mexican Hat is fairly smooth, and generically has a single minimum. The most important effect of the realization-dependent terms is to allow for symmetry-breaking even for finite g . *Therefore, both disorder and interactions are crucial to this symmetry-breaking: Interactions produce the Mexican Hat potential causing spontaneous symmetry-breaking at $g = \infty$, while explicit sample specific symmetry breaking terms prevent the restoration of symmetry by quantum fluctuations even at finite g .*

At $T = 0$ one can simply evaluate the fermionic ground state energy $\mathcal{E}_F(\sigma)$ corresponding to each static σ numerically. We show the resulting effective potential of Eq. (93) in Fig. 6 for the illustrative case $m = 2$. As can be seen, there is an approximate Mexican Hat circle of degenerate minima. In Fig. 7 we zoom in on this circle to see that the degeneracy is broken by sample-specific disorder and that the fluctuations are indeed of order $1/g$ relative to the self-averaging term. Clearly, the numerical work corroborates the analytical picture developed above.

One can now ask how various measurable quantities behave in the strong-coupling phase. There are three such quantities of interest.

³The low frequency approximation $f(\omega) \simeq \omega^2/(4\Delta)$ tracks the exact expression to within ten percent in this range.

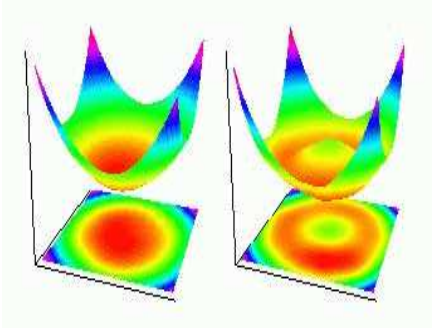


FIG. 6. The effective potential as a function of σ for $m = 2$, with $g = 20$ and $u_m = -1.2$ (left panel) and $u_m = -1.7$ (right panel). The symmetry-breaking in the second case is clear.

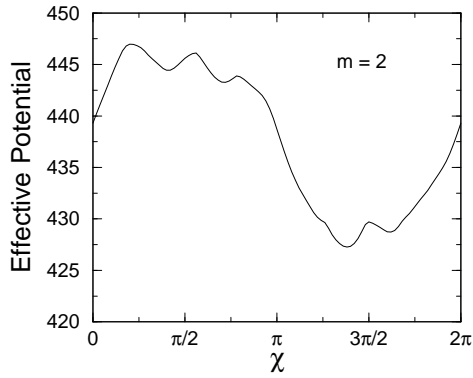


FIG. 7. The effective potential in the Mexican Hat in units of Δ plotted as a function of the angle χ for $m = 2$, at $g = 20$ and $u_m = 1.7$. Note the single nondegenerate minimum and the scale of sample specific disorder, which is of order $1/g$ relative to the average.

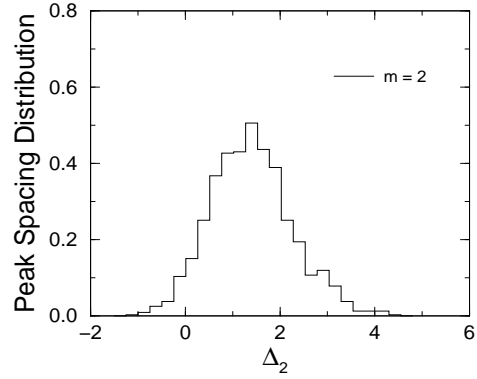


FIG. 8. The peak-spacing distribution for $m = 2$, at $g = 20$ and $u_m = 1.7$. Note the incidence of negative values of the peak-spacing, which is impossible in a noninteracting model.

- The addition spectrum, which measures the difference in ground state energies $\Delta_1(N) = \mathcal{E}_{N+1} - \mathcal{E}_N$ where the total energy of the system with N particles \mathcal{E}_N is the sum of the fermionic energy and the energy of the bosonic field σ (Eq. (95)). We have not included the charging energy $U_0 N^2/2$. The Coulomb Blockade peak spacing is then given by $\Delta_2(N) = \Delta_1(N+1) - \Delta_1(N)$.
- The peak-height distribution.
- The persistent current in response to an external flux.

Since at any particular σ the electronic excitations are controlled by a single-particle Hamiltonian, and σ is well-localized, one might naively imagine that the addition spectrum is the same as the level-spacing spectrum, which is the Wigner-Dyson distribution with an enhanced Δ . However, this ignores possible shifts of σ upon adding a particle. Most of the time the value of σ shifts only a little upon adding a particle. However, every now and then a minimum which was far away in σ -space becomes lower upon adding a particle. One can compute the peak spacing from $\Delta_2(N) = \Delta_1(N+1) - \Delta_1(N)$. In Figure 8 we show the distribution of Δ_2 calculated numerically by the method explained above Eq. (94). As can be seen, negative values of Δ_2 are possible because of the rare events in which σ changes discontinuously upon adding a particle, which makes the distribution broader and more symmetric than the level-spacing distribution. (Note once again that the negative answer results only upon subtracting out the charging energy U_0 .) In contrast negative values of Δ_2 are impossible in a noninteracting model.

Now consider the peak heights. In the noninteracting case, the distribution has been computed in RMT by Jalabert, Stone, and Alhassid³⁹, and measured experimentally in the weak-coupling regime at very low temperatures⁴⁰. There are characteristic differences³⁹ between the peak-height distributions for the GOE (time-reversal unbroken) and GUE (time-reversal broken) which have been measured⁴⁰, and will play a role in the following subsection. There are discrepancies be-

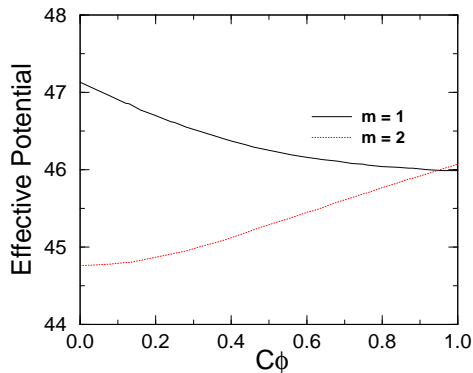


FIG. 9. The ensemble-averaged ground state energy as a function of external flux for $m = 1$ (solid line) and $m = 2$ (dashed line), at $g = 20$ and $u_m = 1.7$. Note the fact that the ground state energy increases for $m = 2$, which thus shows diamagnetic behavior, while $m = 1$ shows paramagnetic behavior.

tween theory and experiment at higher temperatures⁵⁰ which we will address qualitatively in a later subsection. As long as σ changes by small amounts when particles are added the strongly-coupled system behaves much like the noninteracting system. However, when a large change of σ is involved, all the electrons must change their state to adjust to the new σ . This means the transition matrix element the fermion creation operator between the two ground states will be small, and we expect the peak height to be considerably smaller.**This effect produces a correlation between smaller than average *peak spacing* and small *peak height*.

Finally, let us briefly consider the response of the system to an external flux, leaving the details to Part II¹¹ (a short report of this work can be found in ref.¹²). This response is none other than the persistent current

$$I_{pers} = -\frac{\partial F}{\partial \phi} \quad (102)$$

where F is the Free energy (the ground state energy at $T = 0$). This response is primarily orbital in *GaAs* due to the tiny coupling of the external flux to the spins.

Figure 9 shows the ground state energy as a function of external flux averaged over many disorder realizations. The noteworthy point is that the average persistent current is diamagnetic. To see why this is special, a brief digression into what is known about persistent currents is necessary. In a mesoscopic ring penetrated by a flux, the ground state energy has to be periodic in the flux, since an integer number of flux quanta can be gauged away. So

**Changing σ is the same as changing a parameter in a non-interacting random Hamiltonian, a theme which has been explored in the literature⁶¹. Borrowing the result for the overlap of determinants⁶², for ground states differing by $\delta\sigma$ we expect the peak height to scale as $e^{-g \ln g (\delta\sigma)^2}$.

$$I_{pers}(\phi) = -\frac{\partial F}{\partial \phi} = I_1 \sin(2\pi\phi/\phi_0) + I_2 \sin(4\pi\phi/\phi_0) + \dots \quad (103)$$

where $\phi_0 = h/e$ is the flux quantum.

The noninteracting problem is relatively well-understood^{2,51}. Only the even moments I_{2n} survive disorder-averaging (this result holds for the interacting case as well). The *typical*, fluctuating values of the Fourier coefficients are (for small n) $I_{n,typ} \approx E_T/\phi_0$ while the average is $\langle I_{2n} \rangle \approx \Delta/\phi_0$.

Interactions, when included in renormalized first-order perturbation theory³², produce

$$\langle I_2 \rangle \approx \mu^* \frac{E_T}{\phi_0} \quad (104)$$

where μ^* (typically < 1) is the dimensionless Cooper-channel interaction at low energies. The conclusion is that interactions enhance the average persistent current, but that if $\mu^* > 0$ $\langle I_2 \rangle$ should be paramagnetic, while if $\mu^* < 0$ it should be diamagnetic. Much numerical work has followed since⁵², mostly on one-dimensional rings, confirming that interactions do indeed enhance $\langle I_2 \rangle$ in the spinful case.

Experiments⁸ reveal striking discrepancies with the above predictions. The predicted value³², while of the right order-of-magnitude, is still smaller than experiment. More disturbingly, *the sign is inconsistent*. Even materials that show no sign of superconductivity (implying that $\mu^* > 0$) show⁸ a diamagnetic $\langle I_2 \rangle$. Many other explanations (e.g. ref.^{53,54}) have been proposed to account for these observations, but questions about the sign and the magnitude of persistent currents in non-superconducting materials remain open³³.

In this context it is striking to obtain, as we do for m even, a diamagnetic persistent current in a model without superconductivity.

All the signatures described above (except for the diamagnetic persistent current) also hold for the case of m odd. However, there are further interesting effects which we describe below.

2. The Case of m Odd

Let us now turn to odd m , where the first-order contribution in σ to the effective potential is missing. In fact, one can show a much more general result, that the ground state energy to all orders $\mathcal{E}(\chi)$ at a particular angle χ with $\sigma = |\sigma|$ fixed satisfies

$$\mathcal{E}(\chi) = \mathcal{E}(\chi + \pi) \quad (105)$$

To show this result we write the second-quantized fermionic Hamiltonian for the illustrative case of $m = 1$ as

$$H_F(\chi) = \sum_{\alpha} \varepsilon_{\alpha} c_{\alpha}^{\dagger} c_{\alpha} - g \Delta \sigma \sum_{\alpha, \beta, \mathbf{k}} c_{\alpha}^{\dagger} c_{\beta} \phi_{\alpha}^{*}(\mathbf{k}) \phi_{\beta}(\mathbf{k}) \cos(\theta - \chi) \quad (106)$$

and its first-quantized version:

$$h_{\alpha\beta} = \delta_{\alpha\beta}\varepsilon_{\alpha} - g\Delta\sigma \sum_{\mathbf{k}} \phi_{\alpha}^*(\mathbf{k})\phi_{\beta}(\mathbf{k}) \cos(\theta - \chi). \quad (107)$$

Using Eqs. (32,98) along with $\theta(-\mathbf{k}) = \theta(\mathbf{k}) \pm \pi$ one can easily show that

$$h^*(\chi) = h(\chi + \pi) \quad (108)$$

Since the Hamiltonian is hermitian at every χ its eigenvalues are real, and thus

$$\begin{aligned} h(\chi)\Phi_n(\chi) &= \epsilon_n(\chi)\Phi_n(\chi) \\ \Rightarrow h^*(\chi)\Phi_n^*(\chi) &= \epsilon_n(\chi)\Phi_n^*(\chi) \\ \Rightarrow h(\chi + \pi)\Phi_n^*(\chi) &= \epsilon_n(\chi)\Phi_n^*(\chi) \end{aligned} \quad (109)$$

which shows that all the single-particle energies of $h(\chi)$ are shared by $h(\chi + \pi)$, so naturally the ground state energies are the same as well. This implies that the energy as a function of angle χ generically has two exactly degenerate minima. The complex conjugate relationship between the single-particle wavefunctions shows that the two minima are connected by a time-reversal transformation \mathcal{T} . This is easy to understand for $m = 1$. In the bulk an $m = 1$ distortion is just a shift of the Fermi surface. Since the underlying Hamiltonian is time-reversal symmetric, any distortion should have the same energy as the time-reversed distortion.

It is also important to understand that an $m = 1$ distortion in the quantum dot does not represent a current flowing in a particular direction, as it would in the bulk: This is impossible in the steady state in a closed dot. Rather, the $m = 1$ distortion describes a persistent circulating current within the dot. One can understand this by referring to Eq. (29), which shows that the state we label by \mathbf{k} in the dot has a vanishing wavefunction at the boundary (assuming a hard wall boundary condition for simplicity), and therefore the current carried by it vanishes at the boundary of the dot.

Once again, one can numerically corroborate all these deductions, as shown in Figs. 10 and 11, which show the approximate Mexican Hat and the double-degeneracy in it for the illustrative case of $m = 1$.

Similarly, the peak-spacing distribution can also be numerically obtained, as shown in Fig. 12.

Thus, the $O(2)$ symmetry of the Mexican Hat in the $g = \infty$ limit is broken down to a two-fold degeneracy for any finite g . This leads to a very interesting physics which depends sensitively on the coupling to the leads.

Isolated Dot

The isolated dot has two exactly degenerate minima in the effective potential. However, the low-energy dynamics of σ will induce a ‘‘tunneling’’ term between the two minima. Recall that the ‘‘kinetic’’ part of the effective action at very low energies was approximately

$$S_{eff,kin} = g \int d\tau \left(\frac{d\sigma}{d\tau} \right)^2 \quad (110)$$

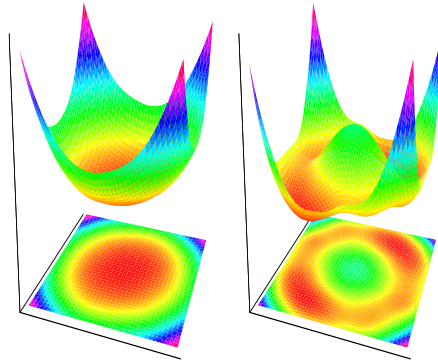


FIG. 10. The effective potential as a function of σ for $m = 1$, with $g = 20$ and $u_m = -1.2$ (left panel) and $u_m = -1.7$ (right panel).

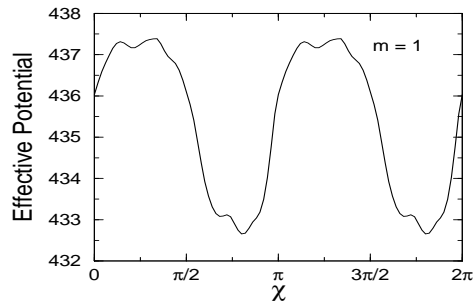


FIG. 11. The effective potential in the Mexican Hat in units of Δ plotted as a function of the angle χ for the case $m = 1$, at $g = 20$ and $u_m = 1.7$. Note the exact two-fold degeneracy of the effective potential minima, and the scale of sample specific disorder, which is of order $1/g$ relative to the average.

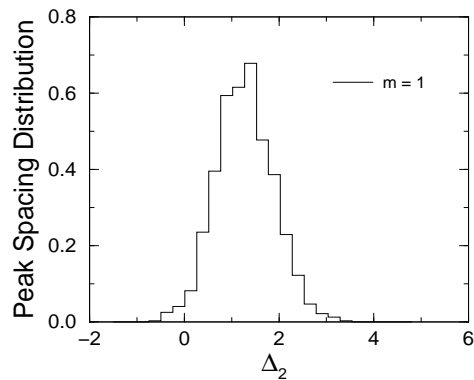


FIG. 12. The peak-spacing distribution for $m = 1$, at $g = 20$ and $u_m = 1.7$. Note the incidence of negative values of the peak-spacing, which is impossible in a noninteracting model.

The tunneling amplitude typically goes as

$$A = e^{-\int dx \sqrt{2mV(x)}} \quad (111)$$

where the integral is over the classically forbidden region. In this problem the mass, read off from the kinetic term, is of order g , and so is the potential in the angular direction. Thus the tunneling amplitude must be of order Δe^{-g} .

Thus the true eigenstates of the system will be the symmetric superposition, which is the ground state, and the antisymmetric superposition which is the excited state. The splitting between them will be of order $e^{-g}\Delta$. The ground state at $T = 0$ will not have any symmetry-breaking.

However this state of affairs describes a very narrow low temperature range: For $\Delta \gg T \gg e^{-g}\Delta$ the system will be in an (essentially) equal incoherent mixture of the symmetric and antisymmetric states, or equivalently, by change of basis, in an equal incoherent mixture of the two minima of the effective potential. Each of these minima has \mathcal{T} -broken dynamics and GUE statistics^{39,40} *even in the absence of an external magnetic field*. Since the two minima have complex conjugate wavefunctions, the incoherent average will wipe out the the persistent currents which change sign under complex conjugation, but not the GUE peak-height statistics³⁹ which are immune to complex conjugation.

Another way, besides increasing T to experimentally observe this degeneracy is to explicitly break time-reversal symmetry by introducing a small external magnetic flux ϕ . The response of the system to such a flux will be linear instead of quadratic, as in the time-reversal invariant cases. here are some specifics.

The flux is introduced within the theory by replacing the non-interacting part of the Hamiltonian by one drawn from an ensemble of crossover Hamiltonians¹⁴. Including the external flux, the first quantized Hamiltonian at a particular angle χ is (from Eq. (106))

$$h = h(\chi) + \frac{C\phi}{\phi_0} h_A \quad (112)$$

where C is a constant of order unity that depends on the shape of the dot and the nature of boundary scattering²¹, and h_A is an appropriately normalized, random, pure imaginary, antisymmetric matrix in any orthogonal basis¹⁴ with typical matrix elements of size $\Delta\sqrt{g}$. It is easy to show that the two minima of V_{eff} move in opposite directions to first order in ϕ . It is convenient to use the exact noninteracting eigenstates as a preferred orthogonal basis. Using the notation of Eq. (109), the change in energy to first order is

$$\delta\mathcal{E}_F(\chi) = \sum_{n \text{ occ}} \sum_{\alpha\beta} (\Phi_{n,\alpha}(\chi))^* h_{A,\alpha\beta} \Phi_{n,\beta}(\chi) \quad (113)$$

where $\Phi_{n,\alpha}(\chi)$ is the projection of the n^{th} exact eigenfunction of Eq. (112) on the noninteracting disorder eigenvector α . Noting from Eq. (109) that $(\Phi_{n,\alpha}(\chi))^* =$

$\Phi_{n,\alpha}(\chi + \pi)$, and using the antisymmetry of h_A in the basis of exact noninteracting eigenstates, it follows that

$$\delta\mathcal{E}_F(\chi) = -\delta\mathcal{E}_F(\chi + \pi) \quad (114)$$

One can estimate the magnitude of $\delta\mathcal{E}_F$ by squaring and averaging over the ensemble to be $\delta\mathcal{E}_F \simeq (g\Delta)\phi/\phi_0$. When this energy exceeds the splitting between the symmetric and antisymmetric states, the system will localize σ in the lower minimum of V_{eff} , thus breaking time-reversal symmetry completely. The flux needed to achieve this at $T = 0$ is known as the crossover flux

$$\phi_{cross} \simeq \phi_0 e^{-g}/g \quad (115)$$

which is exponentially small in g . The effective schematic hamiltonian in the subspace of the two minima, labeled + and - is of the form

$$\Delta \begin{pmatrix} bg & e^{-g} \\ e^{-g} & -bg \end{pmatrix} \quad (116)$$

where b denotes the external magnetic field and Δe^{-g} the tunneling amplitude between the two minima related by time-reversal.

This response to an applied flux should be contrasted with the noninteracting case, when the crossover flux (for single-particle properties) is of the order of ϕ_0/\sqrt{g} . The persistent current in the m odd case is paramagnetic¹², as can be seen from Fig. (9). The ground state energy decreases linearly for small ϕ , a consequence of the first order contribution.

The response of the time-reversal broken system manifests itself in the shift in the zero-bias conductance peak position as a function of external flux. Since the peak position reflects the difference $\Delta_1 = \mathcal{E}_{N+1} - \mathcal{E}_N$, and all the single-particle energies change *linearly* with flux (for $\phi_0/\sqrt{g} \gg \phi \gg \phi_{cross}$), the shift in the peak position must also be linear in the external flux. This contrasts with the noninteracting case where the shift is quadratic in the external flux for $\phi_0/\sqrt{g} \gg \phi$. The numerical results are shown in Fig 13.

For $\Delta \gg T \gg e^{-g}\Delta$ one can carry out a linear-response magnetization measurement, about which more will be said in Part II¹¹. The two degenerate states will lead to a $1/T$ Curie-like linear response. Let us now turn to what happens when the quantum dot is weakly coupled to the leads.

Dot Coupled to Leads: Mapping to the Caldeira-Leggett and Kondo Problems for m odd

We have already seen that at very low energies the dynamics of σ in an isolated dot becomes Hamiltonian, due to the fact that there are no particle-hole excitations below a lowest energy. This changes if the dot is coupled to leads, since the dot levels will hybridize with the continuum of levels in the leads. This leads to dissipative dynamics for σ at arbitrarily low energies. Since in the case of m odd we know that there are two degenerate minima of the effective potential, we are naturally led to

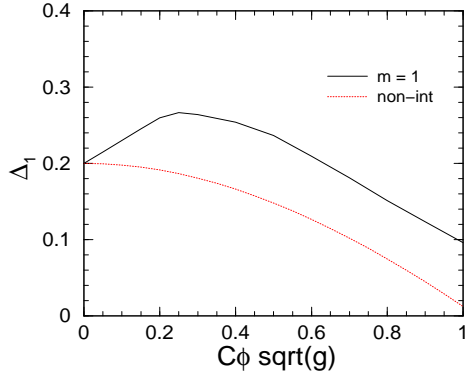


FIG. 13. The peak position $\Delta_1 = \mathcal{E}_{N+1} - \mathcal{E}_N$ as a function of external flux in the range $0 < C\phi < \phi_0/\sqrt{g}$ for $m = 1$, at $g = 50$ and $u_m = 1.7$. Note the fact that the peak position is linear in the flux for small values of flux in contrast to the noninteracting result (dashed line) which is quadratic.

the Caldeira-Leggett problem³⁴, which concerns a particle in a degenerate double-well potential interacting with a “bath” of harmonic oscillators which model the dissipation. Applying the solution^{35,36} of the Caldeira-Leggett model to our problem, *we can predict that there will be two phases depending on the strength of the coupling to the leads: One with spontaneously broken time-reversal symmetry where the σ field is trapped in one minimum, and one where it can successfully tunnel back and forth between the two minima and time-reversal symmetry is unbroken.*

Let us recall some of the principal results of Caldeira and Leggett³⁴. Their motivation was to study systems with a macroscopic quantum mechanical degree of freedom (such as the flux through a superconducting loop or σ in our case) coupled to a dissipative environment. If the particle is initially set up to be in the lowest state of a single well, in the absence of dissipation the particle will eventually tunnel between the minima, with the ground state being a symmetric superposition of the lowest states of the two wells. In the presence of dissipation tunnelling becomes sensitive to the spectral density of the harmonic oscillator bath at low frequencies. For the case of ohmic dissipation, Caldeira and Leggett concluded³⁴ that dissipation decreases the tunnelling rate.

Soon after this, Chakravarty³⁵ and Bray and Moore³⁶ took the results much further. They pointed out a deep connection between this problem and the anisotropic Kondo problem⁵⁵ of electrons interacting with a localized spin. They reached the important conclusion that there are two phases in the Caldeira-Leggett problem. At sufficiently weak dissipation the particle is delocalized between the two degenerate wells, and this corresponds to the Kondo singlet phase of the antiferromagnetic Kondo model ($J_\perp > 0$). At strong dissipation the particle is localized in one well, corresponding to the ferromagnetic Kondo model ($J_\perp < 0$), for which the spin-flip terms are irrelevant at low energies.

The relation of this work to ours is made more precise if we consider the effective action⁵⁶ used by

Chakravarty³⁵ for a resistively shunted superconducting quantum interference device (SQUID):

$$S_{eff} = \frac{\beta\hbar}{\hbar} \int_0^{\beta\hbar} dt \left[\frac{\hbar^2 C}{8e^2} \left(\frac{d\theta}{dt} \right)^2 + u(\theta) \right] + 2\eta \int_0^{\beta\hbar} \frac{dt dt'}{(t-t')^2} \sin^2 \left(\frac{\theta - \theta'}{4} \right) \quad (117)$$

where θ denotes the flux (in units of $\phi_0/(2\pi)$), C is the capacitance of the SQUID, $u(\theta)$ is the double-well potential with degenerate minima at $\pm\theta_0$, and the dimensionless number $\eta = \hbar/2\pi e^2 R$ parameterizes the dissipation (R is the shunt resistance). The phase transition occurs³⁵ (in the limit when the tunnelling amplitude is very small) for $4\eta \sin^2(\theta_0/2) = 1$. The effective action for the Kondo problem⁵⁵ can also be cast in the above form.^{††}

In our problem, dissipation at very low frequencies will enter the effective action through the susceptibility, which is the quadratic term in σ in the fermionic $TrLn$. We have seen before (Eqn. (88)), in the case of the isolated dot, that the dynamics of σ become dissipative for $\omega \gg \Delta$ when it can decay into numerous fermionic many-body states. When connected to the leads, this Landau damping behaviour persists down to the Fermi energy because the dot states are now embedded in the continuum and $A_\alpha^{p,h}$, the spectral densities of the state labelled by α above (p for particle) and below (h for hole) the chemical potential in the exact basis, evolve from the delta function to a Lorentzian of width Γ .

$$A_\alpha(\varepsilon) = \Theta(\varepsilon)A_\alpha^p(\varepsilon) + \Theta(-\varepsilon)A_\alpha^h(\varepsilon) = \frac{\Gamma}{\Gamma^2 + (\varepsilon - \varepsilon_\alpha)^2} \quad (118)$$

Since we are focusing on very low frequencies, the spectral densities are of order Γ/Δ^2 . Remembering that $|M_{\alpha\beta}|^2$ is typically of order $1/g$, and putting in the overall factor of g^2 in the quadratic term, one can easily check that the imaginary part of the susceptibility which represents dissipation will therefore be of order $g\Gamma^2\omega$. Going over to the imaginary time representation, one can show that up to an unimportant constant we have the following term in the effective action

$$g \frac{\Gamma^2}{\Delta^2} \int_{-\infty}^{\infty} \frac{d\omega}{2\pi} |\omega| \sigma(\omega) \cdot \sigma(-\omega) = \frac{2g\Gamma^2 \langle \sigma \rangle^2}{\pi \Delta^2} \int \frac{dt dt'}{(t-t')^2} \sin^2 \left(\frac{\chi - \chi'}{2} \right) \quad (119)$$

^{††}The dissipation induced by the bath manifests itself as a long-range $1/|t - t'|^2$ interaction in Euclidean time. Exactly the same effective action is obtained by integrating out the dissipative electrons in the Kondo problem, as was done by Anderson, Yuval, and Hamann⁵⁵. At a physical level, the particle spends most of the (Euclidean) time in one of the wells, occasionally tunnelling between them, an event called an instanton. These instantons correspond to spin-flip events in the Kondo problem⁵⁵.

In addition we also have the $\left(\frac{d\chi}{dt}\right)^2$ term from the higher energy states.

Comparing our full effective action (Eq. (87) + Eq. (119)) to that of Chakravarty³⁵ (Eq. (117)), we see that the angle χ of σ corresponds to the “particle” degree of freedom θ , and that $g\Gamma^2/\Delta^2 \approx 1$ corresponds to large dissipation (in the strong coupling phase $\langle\sigma\rangle$ is of order unity). Therefore, despite the fact that the two minima are exactly degenerate, σ will be localized in a single minimum at large g for $\Gamma > \Delta/\sqrt{g}$. Even when this condition is satisfied the level width is still much smaller than the level spacing for large g . Under these conditions time-reversal symmetry will be spontaneously broken for m odd and zero temperature. As mentioned before, time-reversal symmetry breaking can be inferred from the statistics of peak heights^{39,40}. This symmetry-breaking also induces a spontaneous persistent current at zero flux, and will be described in Part II¹¹. Note however that in order to see this effect we need $T < \Delta e^{-g}$ since above this T , thermal effects will produce the same effect.

The \mathcal{T} -breaking transition is structurally identical to the ferromagnetic-antiferromagnetic Kondo transition, but is different in character from other Kondo-like states proposed in quantum dots^{57,58}. Any Kondo-like state has to start from a finitely-degenerate set of states forming a pseudospin, and “conduction” electrons with a continuum of energies coupling to this pseudospin. The two main previous proposals are: (i) The degeneracy is in the number of particles at the zero-bias conductance peak, when the dot has the same free energy to have N or $N+1$ particles, which are the two states of the pseudospin- $\frac{1}{2}$. Electrons hopping from the leads “flip” the pseudospin, and at low enough T form a Kondo resonance at the Fermi energy⁵⁷. (ii) A dot with an odd number of electrons has a singly-occupied state as the highest occupied level with spin- $\frac{1}{2}$, which then acts as a standard Kondo impurity⁵⁸. In both these examples, one cannot change the sign of the Kondo coupling to go from the antiferromagnetic to the ferromagnetic Kondo model. Thus, while there is an observable resonance at the Fermi energy below the Kondo temperature T_K , there is no phase transition (see, however, Ref.⁵⁹). The new features of our state are that the pseudospin is a truly collective variable, which represents the Fermi surface distortion of all the electrons, and that one can drive the transition between the analogs of the antiferromagnetic and ferromagnetic Kondo problem merely by tuning the coupling to the leads. In contrast to the $g = \infty$ mesoscopic Pomeranchuk transition which broadened into a crossover for any finite g , this is a true quantum phase transition. The finite system is able to do this by coupling coherently to the infinite reservoir via the leads.

B. The Quantum Critical Regime

Now we turn to a description of the quantum critical regime, which can be reached from the strong- or the

weak-coupling regimes by increasing either the probe frequency, gate voltage, temperature T or $1/g$. We will focus below on increasing $1/g$.

The most important feature of this regime is that σ has a gap of order Δ whereas in the weak-coupling regimes it has a gap of order $g\Delta$. This in turn leads to a broad spectral function for low-energy excited states. This could be seen in tunnelling at finite bias⁶⁰ (nonlinear conductance).

1. Connection to Fock-Space Delocalization

The physics of the quantum critical regime can be connected to ideas of Fock-Space localization-delocalization^{37,38}, which examine the spectral function of an excited quasiparticle state in a mesoscopic system as interactions are turned on. Assuming no correlation between the matrix elements of the interaction, $V_{\alpha\beta\gamma\delta}$, these studies concluded that for excitation energy

$$\varepsilon \geq \varepsilon^* \approx \Delta\sqrt{g/\ln g} \quad (120)$$

the spectral function of the quasiparticle is broadened into a Lorentzian, characteristic of the infinite system. Below ε^* the spectral function splits up into a number of sharp peaks. We briefly recount the simple arguments behind this result (modulo the $\ln g$)³⁷ as it relates also to our work. Consider a single particle of energy ε decaying into a particle of lower energy and a particle-hole pair by Fermi’s golden rule. By energy conservation we need only consider the energy of the particle-hole pair as independent. The matrix element for the process is $V_{\alpha\beta\gamma\delta} \simeq \Delta/g$, while the density of states is just the density of particle-hole states (or two-body states), which is given by the number of ways of partitioning the total energy ε among three particles $\nu_3(\varepsilon) = \varepsilon^2/2\Delta^3$. Note that this is much smaller than the density of many-body states. The total width induced by this process is roughly $\Gamma \simeq \varepsilon^2/g^2\Delta$. If this is much smaller than Δ one cannot make the continuum approximation, and the quasiparticle weight will split into a number of sharp peaks. The correct criterion is to compare the matrix element between two different three-body states $|u_m|\Delta/g$ to the typical spacing between such states $1/\nu_3(\varepsilon)$. If the two are comparable, the quasiparticle weight gets distributed among many such states. This leads to the criterion $\varepsilon^* \simeq \Delta\sqrt{g}$. To obtain the extra $\ln g$ in Eq. (120) requires a more sophisticated analysis³⁷, in which Fock-Space is thought of as a lattice, each site of which corresponds to a single Slater determinant. Hopping on the lattice is accomplished by the interaction matrix elements $V_{\alpha\beta\gamma\delta}$. If the system is localized on this lattice, then the quasiparticle state is comprised of at most a few determinants, and the spectral function will therefore be a sum of sharp peaks. If the system is delocalized on this lattice, the quasiparticle state has an infinite number of Slater determinants, and the spectral function is broadened into a Lorentzian. To find the threshold energy for delocalization ε^* one carries out the analog of the Anderson locator expansion.

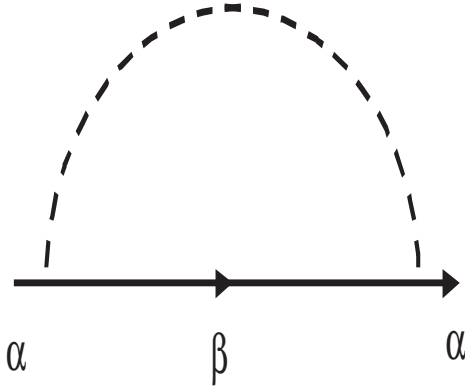


FIG. 14. The lowest-order self-energy diagram for the fermion due to its coupling to the collective field σ . Straight lines represent fermions while wavy dotted lines represent σ .

Let us see how this gets modified in our approach wherein we keep correlations between different $V_{\alpha\beta\gamma\delta}$ (all of which really arise from a single Landau parameter). This gives rise to loop corrections which were neglected earlier^{37,38}, which lead at the critical point to $V_{\alpha\beta\gamma\delta}$ which increase as the energy scale is lowered, as discussed in Section III. In fact, the Fermi-surface distortion becomes the bosonic dynamical variable σ , which interacts with the fermion to give it a decay width.

To make this more quantitative, let us consider the retarded, real-time, inverse propagator of σ (after self-averaging the wavefunction sums) in the weak-coupling phase

$$D_{ret}^{-1}(\omega) = \frac{g^2\Delta}{|u_m|} - \frac{g\Delta^2}{2} \sum_{\alpha\beta} \frac{N_\beta - N_\alpha}{\varepsilon_\alpha - \varepsilon_\beta - \omega - i\eta} \quad (121)$$

where η is a small positive infinitesimal.

The fermions couple to σ through the term $-g\Delta\sigma \cdot \mathbf{M}$ (Eq. (78)). The fermion propagator will get dressed by this coupling, and acquire a self-energy $\Sigma_{ret,\alpha}$, the simplest diagram for which is shown in Fig. (14). The decay width produced by this diagram can be written as

$$\Gamma_\alpha(\omega) = -Im\Sigma_{ret,\alpha}(\omega) = g^2\Delta^2 \sum_{\beta} |M_{\alpha\beta}|^2 \times \int_0^\omega \frac{d\omega'}{\pi} Im D_{ret}(\omega - \omega') \times Im G_\beta(\omega') \quad (122)$$

where Im stands for the imaginary part of the function that follows.

In computing the width by the above one loop diagram, we seem to be following standard diagrammatic perturbation theory. There is, however, a subtlety that needs to be borne in mind. The σ propagator we use is the not the bare one based on the last term in the action of Eqn. (78), (where it had no ω dependence) but an effective one Eqn. (88), *obtained upon integrating out the fermions*. One may ask what the fermion is doing in the one-loop graph above if it has already been integrated out. Is there some double-counting? In Appendix B we will show that there is no double-counting and that the

above procedure for finding Γ is legitimate. Appendix B also explains how to incorporate symmetry-breaking (a nonzero average for σ) into the calculation.

Resuming our calculation of Γ , we will assume (and justify later) that the fermion spectral function is still sharp on the scale of a few Δ so that we can make the replacement

$$Im(G_{ret,\beta}(\omega)) \simeq -\pi\delta(\omega - \varepsilon_\beta) \quad (123)$$

inside the integral of Eq. (122). We now consider the spectral function of the σ -propagator. In Eq. (121), for $\Delta \ll \omega \ll E_T$, the ω -independent part of the sum over $\alpha\beta$ produces $g^2/|u_m^*|$, while the dominant ω -dependence is imaginary. Reading off the imaginary part from Eq. (121), we get

$$D_{ret}(\omega) \simeq \frac{2/g\pi}{-i\omega + \zeta} \quad (124)$$

where

$$\zeta = 2rg\Delta/\pi \quad (125)$$

and

$$r = \frac{1}{|u_m|} - \frac{1}{|u_m^*|} \quad (126)$$

is the distance from the critical point. Note that this involves replacing the discrete sum over particle-hole states by a continuum, and will be justified self-consistently in the following. The imaginary part of this retarded propagator is

$$Im(D_{ret}(\omega)) = \frac{2}{g\pi} \frac{\omega}{\omega^2 + \zeta^2} \quad (127)$$

This shows that ζ acts like a gap or a mass for σ , and when $\zeta \rightarrow 0$, σ should become gapless. Substituting Eqs.(123,127) into Eq. (122) we find the decay width to be

$$\Gamma(\omega) \simeq \frac{\Delta}{\pi} \ln(1 + \omega^2/\zeta^2). \quad (128)$$

In the weak-coupling phase at low energies we have $\omega \ll \zeta$. Expanding the \ln and noting that $\zeta \simeq g/|u_m|$, we recover the weak-coupling result. At the critical point one must replace ζ by Δ . This is the infrared cutoff of the theory, signifying the energy below which D_{ret} has no imaginary part. This implies that in the quantum critical regime, putting the particle on shell ($\omega = \varepsilon$), we have

$$\Gamma(\varepsilon) \simeq \frac{2\Delta}{\pi} \ln \varepsilon/\Delta. \quad (129)$$

Now consider for $\Gamma(\varepsilon)$ in the strong coupling phase. We must expand the theory to quadratic order in σ at the saddle point. The fermionic hamiltonian at the saddle point will take the form

$$h_{\alpha\beta} = \delta_{\alpha\beta}\varepsilon_b + g\Delta\sigma_x M_{\alpha\beta}^x \quad (130)$$

where we have chosen the direction of explicit (sample specific) symmetry breaking to be along the x-axis. The fluctuation about this point have a huge gap of order $g\Delta$ the x or radial direction and of order Δ in the y -direction or angular direction.

To proceed, we must first diagonalize h in Eqn.(130) to get new single particle levels, labeled a, b etc. Their spacing will also be order Δ . It is the width of these states that we want to obtain, using the self-energy diagram of Fig. (14). We need couple only σ_y since σ_x is very heavy. The coupling matrix will change from M_x to $U^\dagger M_x U$, where U relates the α, β basis to the a, b basis. We will assume that that the rotated matrices have the same statistical properties as before rotation, up to factors of order unity. The exchanged σ_y propagator will have a mass of order Δ as can be seen from Eq.(92). This results from the fact that motion in the Mexican Hat (a change of σ_y) has an energy cost of only $g\Delta$, as opposed to a cost of $g^2\Delta$ in the weak-coupling regime. In other words, the Goldstone mode of the self-averaged theory acquires a small mass due to sample-specific disorder. The imaginary part of the σ_y propagator will be of the Landau-damped form and we will obtain a $\Gamma(\omega)$ which is essentially the same as Eq.(129). Thus in entire the strong-coupling regime, the quasi-particle width is universal (up to factors of order unity) and of the same form as the quantum critical region. This is the mesoscopic analog of the Non-Fermi-liquid behavior found in the bulk Pomeranchuk phase⁴⁴.

It is very instructive to analyze Eqn.(128) from different points of view and in different limits, since it describes how a very specific and measurable quantity, the quasi-particle width, is affected in a real problem where r, g and Δ are at play.

- (i) First, since in a finite system all many-body states are discrete one should compare the typical spacing of many-body states with another energy scale (such as T , or the level width due to coupling to the leads, or the finite energy resolution of the experiment, see Silvestrov³⁸) to decide whether the width of Eq. (128) is apparent as a continuous spectral function or as a set of sharp peaks with an envelope given by Eq. (128)^{††}.
- (ii) The crossover between the weak-coupling and

^{††}To compute the decay width at nonzero T we should use the formula

$$\begin{aligned}
\text{Im}\Sigma_{ret,\alpha}(\omega) = & -g^2\Delta^2 \sum_{\alpha\beta} |M_{\alpha\beta}|^2 \frac{1}{\pi} \sum \int d\omega' \text{Im}(G_{ret,\alpha}(\omega')) \\
& \left(\Theta(\omega' - \omega)[N_B(\omega' - \omega) + N_F(\omega')] \text{Im}(D_{ret}(\omega' - \omega)) + \right. \\
& \left. \Theta(\omega - \omega')[1 + N_B(\omega - \omega') - N_F(\omega')] \text{Im}(D_{ret}(\omega - \omega')) \right) \quad (131)
\end{aligned}$$

where N_F is the Fermi function and $N_B(\omega) = (e^{\beta\omega} - 1)^{-1}$ is the Bose function.

quantum-critical regimes can be seen in Eq. (128). Note that the decay width could have depended on the dimensionless parameters r and g in an arbitrary way, but in fact does so only through the energy scale $\zeta = 2rg\Delta/\pi$. This behavior is characteristic of systems near a critical point; the right-hand side of Eq. (128) is a scaling function, and the combination ζ is a scaling variable near the quantum phase transition. Since $g\Delta = E_T$, we see that as one approaches the critical point $r = 0$, the threshold energy for quasiparticle broadening ε^* decreases as rE_T . We emphasize that it never reaches zero; at $r = 0$, it assumes a value Δ , the infrared cutoff. Even if one is in the weak-coupling regime, one can probe the physics of the quantum-critical regime by looking at the quasiparticle width at the energy scale $\varepsilon \simeq \zeta \simeq rg\Delta$. In past work^{37,38}, this behavior was expected at $\simeq \sqrt{g}\Delta$. Thus when r falls below $1/\sqrt{g}$, the threshold for such behavior (ill-defined quasiparticle) also drops linearly with r to a scale as low as Δ . In units of E_T , it drops from E_T/\sqrt{g} to E_T/g .

Since our system has three distinct regimes of behavior, it is fair ask how one is to navigate around the phase diagram. One option is to alter the particle density and hence r_s . The above discussion gives us another option: To vary ω or ε . By increasing this variable (say by conducting a finite-bias study of transport⁶⁰) we can pass from the weak-coupling regime to the quantum-critical regime. By contrast, in the strong-coupling regime, the width is always as in the quantum-critical regime. The reason is that the would-be Goldstone mode σ_y has a very small mass (of order Δ) entirely due to the sample-specific disorder. This is evident from the hamiltonian of Eqn. (92) describing fluctuations.

- (iii) Let us contrast the underlying physics of the weak-coupling and quantum-critical regimes. In the weak coupling limit, $\zeta = 2rg\Delta/\pi$ is very large and we regain

$$\Gamma(\varepsilon) \simeq \frac{\varepsilon^2}{g^2}, \quad (132)$$

a result we could get directly by expanding the σ -propagator as

$$\begin{aligned}
D_{ret}(\omega) \simeq & \frac{|u_m|}{g^2} + \frac{2|u_m|^2}{g^3} \times \\
& \sum_{\alpha\beta} \frac{N_\beta - N_\alpha}{\varepsilon_\alpha - \varepsilon_\beta - \omega - i\eta} + \dots \quad (133)
\end{aligned}$$

and carrying through the ω' -integration in Eqn. (122). It is clear that taking higher-order terms in the expansion in powers of u_m lets the incoming particle decay into final states with higher and higher numbers of particles/holes. From our previous large- N analysis we know that the radius of convergence of this expansion is $|u_m^*|$, since there is an instability of the system for $|u_m| > |u_m^*|$.

At the critical point the incoming particle couples with equal ease to many-body states with arbitrarily many particles and holes.

- (iv) The function in Eq. (129) has no suppression with inverse powers of g , in contrast to the weak-coupling expression ε^2/g^2 . This is a result of the σ gap dropping from order $g\Delta$ to Δ as explained in the points made above. On the other hand as a function of ε it grows quite slowly. The logarithmic growth of width with energy justifies the replacement of the fermion spectral function by the delta function (Eq. (123)) since the function it multiplies in the integral is very broad.
- (v) Recall that in writing down Eq. (127) we assumed that the particle-hole states formed a continuum even at low energies. Armed with the decay rate of Eq. (129) we can justify this self-consistently. The self-consistent D_{ret} is given by the inverse of Eq. (121) with the appropriate self-energies put in for ε_α and ε_β . Thus, each sharp pole in D_{ret}^{-1} , formerly at $\varepsilon_\alpha - \varepsilon_\beta$ will now be smeared out over an energy range of order $\Gamma_\alpha + \Gamma_\beta$. If this width is greater than the typical spacing of two-body states (which is $2\Delta^3/\varepsilon^2$) the continuum approximation is valid. It is easy to verify that this holds for energies as low as a few Δ (modulo the caveat in point (i)).
- (vi) In the quantum-critical and strong-coupling regimes we have argued that single-particle states are strongly connected to many-body states at low energies. One signature of this would be the statistics of the many-body states. When a single Slater determinant forms a good description of the ground state, one expects the single-particle levels to obey Wigner-Dyson statistics, while the low-energy many-body states are nearly uncorrelated and obey Poisson statistics. However, in the quantum-critical and strong-coupling regimes we expect the many-body states at low energies (a few Δ but independent of g) to be strongly coupled and therefore obey Wigner-Dyson statistics. In fact, an exact diagonalization study⁶³ is consistent with this picture. Berkovits and Avishai⁶³ find that at small coupling strength the many-body states display Poisson statistics, while at intermediate coupling strength they obey Wigner-Dyson statistics. They also find a reentrance of Poisson statistics at very high couplings, possibly a signature of a Wigner glass regime^{68,69}.

The decay width of the quasiparticles at nonzero energy above the Fermi energy should be visible in nonlinear conductance experiments⁶⁰ (conductance at finite bias).

Finite- T effects in the weak-coupling regime are worth a little more elaboration. Assume that one is in the weak-coupling regime, whose physics is dominated by the

Universal Hamiltonian²⁰. However, there might be observable effects associated with quantum and/or thermal fluctuations of σ on the peak-height distribution. The experiment⁵⁰ shows a narrower distribution than that expected for noninteracting electrons. Many ideas have been offered to account for this discrepancy, including dephasing⁶⁴, the effect of completely random two-body interactions⁶⁵, spin-orbit interactions⁶⁶, and finite temperature and exchange^{23,24}. While all these may be contributing factors, the analysis of Usaj and Baranger²³ and Alhassid *et al*²⁴ including the effects of exchange in the Universal Hamiltonian²⁰ sense, and the effect of nonzero T , seems to be the most comprehensive. However, despite the fact that a larger value of the exchange constant is used²³ than predicted by RPA (which makes the distributions narrower) the experimental distribution is even narrower than the prediction, and the discrepancy increases with increasing T .

In our approach, as T increases, higher energy states of both the fermions and σ are populated, which will modify the imaginary part of the fermion Green's function (Eq. (131)). This in turn can serve as the input to the formula derived by Meir and Wingreen⁶⁷ for the current through a fully interacting region, which in the simplest case of equal couplings to the right and left leads reduces to

$$I = -\frac{2e}{h} \int d\varepsilon (N_{F,L}(\varepsilon) - N_{F,R}(\varepsilon)) \text{Im}(Tr[\mathbf{\Gamma}\mathbf{G}]) \quad (134)$$

where N_F are the Fermi functions of the two leads, $\mathbf{\Gamma} = \mathbf{\Gamma}_L\mathbf{\Gamma}_R/(\mathbf{\Gamma}_L + \mathbf{\Gamma}_R)$ is the level width matrix and \mathbf{G} is the matrix single-particle Green's function (including all many-body contributions).

It is qualitatively clear that as one approaches the quantum critical regime by increasing T or decreasing ζ , the single-particle fermionic states get more and more strongly coupled to many-body states. This will lead to incoherent averaging of the conductance and thus a narrowing of the peak height distribution beyond that implied by the Universal Hamiltonian treatments^{23,24}. A quantitative calculation is beyond the scope of this paper.

C. The Order Parameter and its Fluctuations

We are now in a position to examine the size of the order parameter and its fluctuations in the three different regimes, and to delineate the crossovers between them. Once again, even and odd m turn out to be significantly different, and we will treat them in turn.

In the case of even m a term linear in σ is allowed, and the effective potential is generically of the form

$$V_{eff}(\sigma) = -g\sigma\Delta \cos(\chi - \chi_0) + \frac{1}{2}g^2\Delta r\sigma^2 + \frac{\lambda}{4}g^2\Delta(\sigma^2)^2 + \dots \quad (135)$$

where the first term arises from the realization-specific disorder and the other terms are self-averaging. The

$\cos(\chi - \chi_0)$ is intended to show the explicit breaking of the rotational invariance in σ -space by the sample-specific disorder. By keeping only the terms kept above, and minimizing in the magnitude and angle of σ , it is easy to verify that near the critical point ($r \ll 1$) the average value of the order parameter is the solution to a cubic and has the form

$$\langle \sigma \rangle \simeq g^{-1/3} f(r g^{2/3}) \quad (136)$$

where $f(x)$ is a scaling function which becomes a constant as $x \rightarrow 0$ and behaves as $\sqrt{|x|}$ for large negative x . Thus the order parameter behaves as $g^{-1/3}$ in the quantum-critical regime and crosses over to a $\sqrt{|r|}$ behavior deep in the strong-coupling regime. From Eq. (136) it is clear that the crossover between the weak-coupling and quantum-critical regimes happens for $|r| g^{2/3} \approx 1$ as far as the order parameter is concerned. This applies equally to the quantum-critical to strong-coupling crossover. Note that this is a different crossover than that found in quasiparticle broadening.

For odd m , only even functions of σ are allowed in V_{eff} , even among the realization-specific terms. The effective potential is generically

$$V_{eff}(\sigma) = -g\Delta\sigma^2 \cos 2(\chi - \chi_0) + \frac{1}{2}g^2\Delta r\sigma^2 + \frac{\lambda}{4}g^2\Delta(\sigma^2)^2 + \text{Blockade} \quad (137)$$

For simplicity, we will assume that either a small nonzero external flux selects one of the two degenerate minima in the following. Clearly, the crossover to the quantum-critical regime happens when the self-averaging quadratic term is comparable to the realization-specific term, leading to the criterion $rg \approx 1$. In the quantum-critical regime the order parameter size is of order $1/\sqrt{g}$, while deep in the strong-coupling regime it behaves as $\sqrt{|r|}$.

Let us now look at the fluctuations of the order parameter. In previous work¹⁰ two of us had wrongly stated that quasiparticle broadening was connected to the delocalization of σ . As has been discussed in the previous subsection at some length, quasiparticle broadening in the quantum-critical and strong-coupling regimes is a direct result of the small gap in the σ propagator (of order Δ). However, the fluctuations of σ remain bounded and nearly the same in all three regimes. To see this, let us calculate

$$\langle \sigma^2(t) \rangle = \int_0^{g\Delta} \frac{d\omega}{2\pi} D(\omega) \quad (138)$$

where D is the Euclidean propagator of σ . Here we have cut off the frequency integration at $E_T = g\Delta$, because retaining higher frequencies would be inconsistent with our starting point, in which all states of energy higher than E_T have been integrated out. From Eq. (124) we obtain

$$D(\omega) = \frac{2/g\pi}{|\omega| + \zeta} \quad (139)$$

and thus

$$\langle \sigma^2(t) \rangle \simeq \frac{2}{g\pi} \log \left[\frac{g\Delta}{\zeta} \right] \quad (140)$$

In the weak-coupling regime $\zeta \simeq rg$, and the size of the σ fluctuations is $1/\sqrt{g}$. This increases a little in the quantum-critical and strong-coupling regimes (where $\zeta \simeq \Delta$) to $\sqrt{\log g/g}$. To reiterate, Fock-space delocalization has to do with the *gaplessness* of σ , and has no relation to its fluctuations.

D. Summary of Signatures and Connection to Experiments

Since this section has been rather long and involved, it is appropriate to collect in this subsection the signatures of the existence of the collective variable in the various regimes. We remind the reader that we have restricted attention to charge-channel instabilities for spinful electrons, in which the spin index is a passive spectator. This restriction is not unreasonable in the light of the values of the Landau parameters⁴² for $r_s = 5$ (Eq. (21)). We emphasize that only the signatures pertaining to Coulomb Blockade are discussed in detail in this paper. Other equally striking signatures in the persistent current will be explored exhaustively in Part II¹¹.

- Strong-coupling regime for all m : σ is localized in a single minimum for m even, or a pair of minima related by time-reversal for m odd, with the size of $|\sigma|$ being of order unity. The addition spectrum and therefore the conductance peak-spacing distribution are broader and more symmetric than the GOE level spacing distribution. This results from rare large shifts of σ as particles are added, which also leads to a correlation between small peak-spacing and exponentially small peak height. The m even case has a diamagnetic persistent current¹² in response to an external flux, while the m odd case has a paramagnetic persistent current. Low-energy quasiparticles are broadened throughout the strong-coupling regime, as will be elaborated below.
- Strong-coupling regime for m odd, isolated dot: At $T = 0$, the system is in a symmetric superposition of two exactly degenerate minima of the effective potential. However, the crossover flux is exponentially small in g , of the order of $\phi_{cross} \approx \phi_0 e^{-g/g}$. The breaking of time-reversal by this tiny flux can be experimentally monitored in the peak-height distribution^{39,40}, which corresponds to the GUE for $\phi > \phi_{cross}$. In the flux regime $\phi_0/\sqrt{g} \gg \phi \gg \phi_{cross}$ the peak position varies linearly with ϕ , in contrast to the noninteracting case in which it would vary quadratically.
- Strong-coupling regime for m odd, dot coupled to leads: The dynamics of σ becomes dissipative at arbitrarily low energies, and our problem can

be mapped on to the Caldeira-Leggett problem³⁴. From its solution^{35,36}, we conclude that at sufficiently high dissipation, corresponding to level widths (due to the dot-lead coupling) of $\Gamma \simeq \Delta/\sqrt{g}$, the system can be driven to spontaneously break time-reversal symmetry. This transition can once again be experimentally accessed via the peak-height distribution^{39,40}, and is isomorphic to a ferromagnetic to antiferromagnetic Kondo transition.

- Quasiparticle width: Throughout the quantum-critical and strong-coupling regimes σ becomes “gapless” in the scaling limit ($g \rightarrow \infty$, $\Delta \rightarrow 0$ with E_T fixed). A single-particle description is no longer valid even at low energies (of order a few Δ), and low-energy quasiparticles are “Fock-space delocalized”. This prediction is in contrast to previous work^{37,38} which suggested a broad quasiparticle only at energies of order $\simeq \Delta\sqrt{g}$. Physically this corresponds to strong mixing between the low-energy single-particle excitations and collective overdamped excitations of σ . In the quantum-critical regime both vector components of σ are gapless, while in the strong-coupling regime, the fluctuations of σ in the nearly degenerate Mexican Hat potential (the would-be Goldstone mode) are nearly gapless.
- Weak-coupling regime: Despite the fact that it is dominated by Universal Hamiltonian physics, quantum and/or thermal fluctuations of σ might have a measurable effect on the width of the peak-height distribution. Such effects are predicted to get stronger as one goes towards stronger coupling (by increasing r_s). The quantum-critical regime can be accessed by measurements at finite bias, nonzero frequency, or nonzero T .

Let us now briefly analyze the relevant experiments. The Sivan *et al*⁵ and Patel *et al*⁶ experiments are done on gated GaAs 2DEG samples, for which $r_s \approx 1 - 1.2$ in the bulk. Using the area of the sample and the fact that these dots are in the ballistic limit we can find both Δ and E_T , and thence find $g \approx 7 - 14$. Sivan *et al*⁵ find that the CB peak spacing is about 5 times broader than that predicted by the Universal Hamiltonian, which describes the weak coupling region of our phase diagram. However, Patel *et al*⁶ find it to be in accord with this prediction, after accounting for “experimental noise” which is determined by measuring the magnetic field asymmetry of the CB spacings (which indicates motion of the dopant atoms, or some other scrambling of the single-particle potential). Thus, the Patel *et al* data seem to lie in the weak-coupling region. The Sivan *et al* data also correspond to the weak-coupling region. Presumably, if the subtraction of experimental noise were to be carried out this data would also match the Universal Hamiltonian predictions.

The experiments by Simmel *et al* and Abusch-Magder *et al*⁶ are performed on Si quantum dots with $r_s \approx 2.2$,

and $g \approx 18$. (For $r_s \geq 2$ local charge density correlations develop in the dot⁶⁸, similar to the classical limit⁶⁹. While a Fermi surface distortion is not a charge density wave, it enhances the susceptibility for one, and could thus be a precursor). Two signatures of the critical fan are found in this experiment⁶. The CB peak-spacing distribution is found to be 7-8 times wider than expected from the Universal Hamiltonian (assuming spin degeneracy). Also, the width of the CB peaks does not vanish⁶ as $T \rightarrow 0$. This is just what is expected for a system was located in the critical fan: The ground and low-lying excited states are “Fock-space delocalized”, and single-particle states are broad even at low energy. However, it is not clear whether the width of the peaks is intrinsic or dominated by charge rearrangement noise⁷⁰.

Finally, as has been discussed in the previous subsection, measurements of the width of the peak-height distribution⁵⁰ and its evolution with T are not completely understood from the Universal Hamiltonian standpoint^{23,24}. Our theory predicts a further narrowing of the peak-height distribution.

In conclusion, current experiments seem to be in the weak-coupling regime, with possible excursions into the quantum-critical crossover at nonzero temperatures. From the values of the Landau parameters for the clean 2DEG⁴² one can guess that systems with r_s substantially larger than 5 will be needed to see the strong-coupling regime, and that charge-channel instabilities are likely to occur first, although occasionally even systems with $r_s = 5$ may happen to be in this regime (see the end of Appendix A). In constructing more strongly interacting sample, one must bear in mind that since $g \simeq k_F L$, reducing the density at constant dot size L will reduce g . What one would ideally like to do is to keep g fixed, which means preparing larger dots while reducing electron density.

VI. CONCLUSIONS AND OPEN QUESTIONS

Starting with the problem of interacting two-dimensional electrons in a ballistic mesoscopic structure with chaotic boundary scattering, we found that Landau Fermi-liquid interactions (parameterized by dimensionless Landau parameters u_m in the m^{th} angular momentum channel) were the most natural starting point at the Thouless scale E_T . The only condition for this to hold is that E_F/E_T be large. For a ballistic/chaotic quantum dot this ratio is of the same order as the dimensionless conductance $g = E_T/\Delta$, where Δ is the mean level spacing. Thus the largeness of g is a sufficient condition for Fermi liquid interactions to be applicable in the Thouless band. This is a new regime in the broad problem of the interplay of interactions and disorder. The special features of this regime which make it controllable are the applicability of Random Matrix Theory, and the presence of the small parameter $1/g$, which conspire to make a large- N ($N = g$) approximation feasible. The solution is nonperturbative in both interaction strength and disorder: The disorder is the strongest it can possibly be,

scattering momentum states chaotically into each other, while the interactions have a dimensionless strength of order unity. The secret to the success of the nonperturbative solution is the additional small parameter $1/g$ which controls the size of fluctuations in the large- N approximation. Note that in contrast to many applications in which the large- N approach is used, in this case it is clearly justified by the largeness of g (5-20 in experimental samples).

Restricting our attention to charge-channel instabilities, we found a disordered version of the Pomeranchuk shape transition in every Landau Fermi-liquid channel, confirming the one-loop RG result found earlier by two of us⁹, and putting it on a rigorous footing as being exact in the large- g limit¹⁰. The corresponding Landau parameter had to be $u_m \leq u_m^* = -1/2 \ln 2 = -0.7213$, as compared to the bulk instability at $u_m \leq -1$. Thus there is a window in which the clean bulk system is stable, but the mesoscopic ballistic/chaotic system is not, which indicates that both interactions and disorder are crucial to the existence of this regime. More specifically, we saw that interactions produce a Mexican Hat potential, and the realization-specific disorder allowed symmetry-breaking even in the presence of finite- g quantum fluctuations. This can be understood as explicit mass generation for the would-be Goldstone mode by sample-specific disorder.

The transition at $g = \infty$ is replaced by a crossover for any finite g . In accord with generally known features of quantum phase transitions³¹ the coupling constant- $1/g$ plane is divided into a weak-coupling regime, a strong-coupling regime, and a fan-shaped quantum critical regime. However, our theory displays additional nontrivial features not found in clean models, such as the persistence of symmetry-breaking even in the zero-dimensional limit, due to sample-specific disorder. In particular, in our theory the shape of the crossover regime depends on the property being considered: For example, the quasiparticle width at low energies has only a single crossover between the weak-coupling and quantum-critical regimes and remains broad throughout the strong-coupling regime. On the other hand, the order parameter displays an additional crossover from the quantum-critical to the strong-coupling regime, with the shape of the crossover depending on whether the angular momentum channel m in which the instability occurs is even or odd. It must be reiterated that these properties can be explicitly calculated in a controllable large- N approximation in all the regimes thanks to the small parameter $1/g$.

Note that we make no attempt to keep all $1/g$ contributions in the effective action S_{eff} , instead keeping only the lowest nontrivial terms of each type. As an example, we do not keep $1/g$ corrections to the self-averaging part of the effective action, but we do keep the $1/g$ terms which break the rotational invariance in σ -space of the self-averaged part, since they have a profound effect on the physics of the strong-coupling regime. Similarly, we keep the “kinetic” terms in S_{eff} which are down by $1/g$ compared to the self-averaging static part of S_{eff} , since

these are the lowest order nonzero terms.

The strong-coupling regime is where the most striking properties of the collective Fermi surface distortion field σ are found. Here a bifurcation occurs with some properties being common to both even and odd m , while others depend on m modulo 2. The features shared by all m in the strong-coupling regime include: (i) A mean value of the order parameter of order unity. (ii) Rare large shifts of the order parameter upon adding a particle, leading to a broadened peak-spacing distribution. (iii) The same phenomenon as (ii) leading to a correlation between small peak-spacing and exponentially small ($\simeq \exp -g \ln g$) conductance due to the near-orthogonality^{61,62} of the states at different $\langle \sigma \rangle$. (iv) Quasiparticles become broad at energies of a few Δ throughout the strong-coupling regime. A special property of the m even strong-coupling regime is a diamagnetic persistent current¹², to be investigated in greater detail in Part II¹¹ of this paper.

The strong-coupling regime of a system with an instability in an odd m channel shows even more striking effects, which depend sensitively on how strongly the dot is coupled to the leads. The physics can be mapped on to the Caldeira-Leggett model³⁴, and is driven by the combination of an exact two-fold degeneracy in the effective potential (a consequence of the time-reversal invariance of the underlying Hamiltonian) and the low-energy dissipation induced by coupling to the leads. At weak dot-lead coupling, the system is “almost” in a time-reversal (\mathcal{T} -) broken state. The crossover flux need to tip the system into a completely \mathcal{T} -broken regime is exponentially small ($\phi_{cross} \simeq \phi_0 e^{-g/g}$), as contrasted with a crossover flux of ϕ_0/\sqrt{g} needed for a noninteracting system. When the dot-lead coupling increases to a value such that the broadening of single-particle states due to the leads reaches $\Gamma \simeq \Delta/\sqrt{g}$, a spontaneous breaking of time-reversal takes place^{35,36}. This is a true quantum phase transition in the universality class of the antiferromagnetic to ferromagnetic Kondo model⁵⁵, and can be achieved by a finite system by coupling coherently to an infinite reservoir. In the \mathcal{T} -broken phase the system also displays a spontaneous paramagnetic persistent current¹² of order E_T/ϕ_0 , to be explored in greater detail in Part II¹¹.

Coming to the quantum-critical regime, the main feature is the “gaplessness” of the collective variable σ , by which we mean that its propagator has the Landau-damped form $-1/i\omega$ for $\Delta \ll \omega \ll E_T$. In this regime low-energy single-particle excitations are strongly coupled to many-body excitations with arbitrary numbers of particle-hole pairs via the collective variable σ . This has many consequences: (i) Recall that the threshold for a continuous and broad spectral function for a particle was found to be $\varepsilon^* \simeq \Delta\sqrt{g/\ln g}$ in earlier work^{37,38} which ignored correlations between interaction matrix elements, and therefore missed the quantum phase transitions found here. In our approach we find that this threshold ε^* decreases to a few Δ independent of g in the quantum-critical regime. This could potentially be seen in nonlinear conductance (conductance at finite bias) experiments⁶⁰. (ii) Since they are strongly

mixed by interaction effects, the statistics of the low-energy many-body states should change in the quantum-critical regime from Poisson towards Wigner-Dyson, as has been seen in recent numerics⁶³ (iii) Finally, and perhaps most relevant for current experiments, one should be able to access the quantum-critical regime from the weak-coupling regime by finite-bias, finite-frequency, or finite-temperature measurements. In particular, there should be a narrowing of the peak-height distribution beyond Universal Hamiltonian effects^{23,24} at nonzero temperature.

As has been mentioned above, the broadening of low-energy quasiparticles persists in the strong-coupling regime due to the near-gaplessness of the would-be Goldstone mode of the Mexican Hat. This seems to be the mesoscopic analog of the non-Fermi-Liquid behavior found throughout the bulk Pomeranchuk phase in clean systems⁴⁴.

Finally, as regards the weak-coupling regime, the collective variable σ has a huge gap here of order rg ($r = \frac{1}{|u_m|} - \frac{1}{|u_m^*|}$ is the distance from the critical point). Thus the weak-coupling regime is controlled by the Universal Hamiltonian²⁰ of Eq. (3), which is the low-energy fixed point in this regime.

The picture that emerges is that just as Landau's Fermi liquid theory is unstable to the bulk Pomeranchuk instability in any Fermi liquid channel, the Universal Hamiltonian is also unstable to the mesoscopic Pomeranchuk instability in any channel, with the instability occurring more readily in mesoscopic ballistic/chaotic systems than in the bulk. The mesoscopic Pomeranchuk regimes represent physics nonperturbatively different from Universal Hamiltonian physics. These strong-coupling regimes, and the crossover quantum-critical regimes, can be accessed by changing the electron density, or temperature, or the probe frequency. The consistency of Random Matrix Theory and large- g enables us to carry out controlled calculations and make predictions in all three regimes. Our analysis provides a new framework for analysing future experiments on strongly interacting mesoscopic systems.

Let us now turn to open questions and possible future directions. Apart from a more precise treatment of finite- T effects²²⁻²⁴ in our theory, the most pressing open question is the treatment of spin-channel instabilities, which necessarily involves the inclusion of the Universal Hamiltonian exchange coupling²⁰ J . In other words, what is the interplay between the mesoscopic Stoner transition²⁰ and the mesoscopic Pomeranchuk transition in a spin channel? One can imagine a cooperative phenomenon whereby the exchange coupling favors symmetry-breaking in a spin Fermi-liquid channel. This might reduce the magnitude of the critical coupling Z_m^* considerably, and hence make the transition observable at smaller r_s . Exotic types of ordering intertwining spin and momentum space indices might also occur⁴³.

A second effect which deserves investigation is the following: We have assumed that no renormalization of the Landau parameters happens at energy scales higher than E_T , whereas they do renormalize below E_T in the man-

ner described in Section III. Clearly, there must be some renormalization of the Landau parameters above E_T , and since the sign of the flow cannot abruptly change, this effect also tends to reduce the critical coupling. To rephrase the question, are the Landau parameters of the chaotic/ballistic cavity the same as those in the bulk 2DEG of the same electron density? Perhaps the best way of resolving this issue is to carry out the analog of the bulk quantum Monte Carlo calculations⁴² directly in a chaotic/ballistic cavity⁷¹.

A somewhat related question concerns slightly diffusive quantum dots, where the bulk mean free path l is smaller than (but not negligible compared to) the size of the dot L . In this case there is an energy regime between $\hbar v_F/L$ and the Thouless energy $E_T = \hbar D/L^2$. In this intermediate energy regime there will be a crossover between bulk diffusive dynamics and Random Matrix dynamics. In the extreme diffusive limit one must recover the Finkelshtein scaling^{45,46}.

One can also ask what happens as one increases the interaction strength (or r_s) to very large values. Is there physics beyond the strong-coupling regimes we have found? Certainly for the Coulomb interaction we know that one must eventually cross over into a Wigner Glass (or Coulomb Glass) regime^{68,69}. The flattening of parts of the Fermi surface in the mesoscopic Pomeranchuk regimes increases the susceptibility for charge density wave instabilities. This indicates that the crossover to the extremely strong-coupling Wigner Glass regime might happen more readily in mesoscopic ballistic/chaotic samples than in bulk disordered samples. An investigation of this crossover would complete the picture of strong-coupling physics in mesoscopic ballistic/chaotic samples.

At a more philosophical level, the identification of a new, controllable, regime of disorder and interactions opens up many possibilities. As an example, one could apply our RG techniques with RMT correlations to the Kondo problem⁵⁵, and investigate the effect of Landau Fermi-liquid interactions between conduction electrons residing in a ballistic/chaotic cavity⁷² on the Kondo effect. Another example to which our techniques might be applied is the effect of Fermi-liquid interactions on granular, disordered, gapless superconductors exhibiting a novel metal-insulator transition⁷³, since the eigenvalue and eigenvector statistics of their grains are expected to be governed by one of four newly discovered RMT universality classes⁷⁴.

To conclude, ballistic/chaotic quantum dots seem to provide us with a unique theoretical and experimental playground with exquisite control on both fronts. On the theoretical front, RMT and the $1/g$ expansion allow us to tackle disorder and interactions simultaneously and nonperturbatively. On the experimental front dots give us the best of both worlds: A phase transition at $g = \infty$ which we can "see" even at finite g and access to all the control parameters a mesoscopic system allows (varying r_s , external flux, bias voltage, and coupling to leads).

We are grateful to the NSF for grants DMR-0071611 (GM), and DMR- 0103639 (RS), DMR-98-04983 (DH and HM), the Aspen Center for Physics for its hos-

pitality, and Yoram Alhassid, Harold Baranger, Sudip Chakravarty, Claudio Chamon, Yuval Gefen, Bert Halperin, Yong-Baek Kim, Eduardo Mucciolo, Chetan Nayak, Yuval Oreg, Zvi Ovadyahu, Boris Shklovskii, Doug Stone, Denis Ullmo, and Chandra Varma for illuminating conversations.

VII. APPENDIX A

In this appendix we will show that the RG equation and the quadratic part of the effective action are self-averaging. Let us first focus on the RG, and look at the part of Eq. (40) which is to be summed over

$$R = \sum_{\nu=-\Lambda}^0 \frac{1}{\Lambda+|\varepsilon_\nu|} \sum_{\mathbf{p}\mathbf{p}'} u(\theta_{\mathbf{k}} - \theta_{\mathbf{p}}) u(\theta_{\mathbf{p}'} - \theta_{\mathbf{k}'}) \times \phi_\mu^*(\mathbf{p}) \phi_\nu^*(\mathbf{p}') \phi_\nu(\mathbf{p}) \phi_\mu(\mathbf{p}') \quad (141)$$

As has been stated before, in RMT the wavefunction averages do not depend on the energy separations of the states, so the wavefunction average can be carried out separately. This average in the GOE for $\mu \neq \nu$ and generic momentum labels is Eq. (41), reproduced below for convenience

$$\langle \phi_\mu^*(\mathbf{p}_1) \phi_\nu^*(\mathbf{p}_2) \phi_\nu(\mathbf{p}_3) \phi_\mu(\mathbf{p}_4) \rangle = \frac{\delta_{14} \delta_{23}}{g^2} - \frac{\delta_{13} \delta_{24} + \delta_{1,-2} \delta_{3,-4}}{g^3} \quad (142)$$

The $1/g^2$ term is the “naive Wick contraction” of leading-order RMT, but the $1/g^3$ term is necessary to maintain orthogonality between μ and ν . The final term would be missing in the GUE. Substituting the correct momentum labels for the particle-hole diagram we see that the wavefunction average is

$$\frac{\delta_{\mathbf{p}\mathbf{p}'}}{g^2} - \frac{1 + \delta_{\mathbf{p},-\mathbf{p}'}}{g^3} \quad (143)$$

Let us first carry out the ensemble average of R . Using Eq. (143) in Eq. (141) we obtain a convolution of the two Fermi liquid functions

$$\sum_{\mathbf{p}} u(\theta_{\mathbf{k}} - \theta_{\mathbf{p}}) u(\theta_{\mathbf{p}} - \theta_{\mathbf{k}'}) = g(u_0^2 + \frac{1}{2} \sum_{m=1}^{\infty} u_m^2 \cos m(\theta - \theta')) \quad (144)$$

where we have reverted to the notation $\theta = \theta_{\mathbf{k}}$, $\theta' = \theta_{\mathbf{k}'}$. Note that we have used

$$\sum_{\mathbf{p}} = g \int \frac{d\theta_{\mathbf{p}}}{2\pi} \quad (145)$$

which is valid for large g . In the second term of Eq. (143), the $\delta_{\mathbf{p},-\mathbf{p}'}$ turns out to be subleading, while the other allows independent sums over \mathbf{p} , \mathbf{p}' . This means that only u_0 contributes due to this term, which produces

$$\sum_{\mathbf{p}\mathbf{p}'} u(\theta_{\mathbf{k}} - \theta_{\mathbf{p}}) u(\theta_{\mathbf{p}'} - \theta_{\mathbf{k}'}) = g^2 u_0^2 \quad (146)$$

Next we need to do the energy sum, which we replace by an integral

$$\sum_{\varepsilon_\nu=-\Lambda}^0 \frac{1}{\Lambda+|\varepsilon_\nu|} \approx \int_0^\Lambda \frac{d\varepsilon}{\Delta} \frac{1}{\Lambda+\varepsilon} = \frac{\ln 2}{\Delta} \quad (147)$$

Putting all the pieces together, we obtain the ensemble average of R to be

$$\langle\langle R \rangle\rangle = \frac{\ln 2}{2g\Delta} \sum_{m=1}^{\infty} u_m^2 \cos m(\theta - \theta') \quad (148)$$

Now consider the fluctuation of the quantity R of Eq. (141), that is, $R - \langle\langle R \rangle\rangle$. Each term in R is of order $1/g^3$, where one factor of $1/g$ comes from the energy denominator, while each wavefunction contributes $1/\sqrt{g}$. There are g^3 such terms coming from the three summations. Since the average has been taken out, each contribution is completely random and comes with a random sign. From a one-dimensional random walk argument, with each step being of size $1/g^3$, and g^3 steps, the net answer must be of order

$$\left(R - \langle\langle R \rangle\rangle \right) \simeq \frac{1}{g^{3/2}} \ll \left(\langle\langle R \rangle\rangle \right) \quad (149)$$

Thus we see that the average of R indeed dominates its fluctuations over the ensemble, and R is therefore self-averaging.

The situation is simpler for the quadratic term of the effective action, Eq. (79) (call it S_2).

$$S_2 = g^2 \sum_{\alpha\beta} \frac{N_F(\beta) - N_F(\alpha)}{\varepsilon_\alpha - \varepsilon_\beta} \sum_{\mathbf{k},\mathbf{k}'} \phi_\alpha^*(\mathbf{k}) \phi_\beta(\mathbf{k}) \phi_\beta^*(\mathbf{k}') \phi_\alpha(\mathbf{k}') (\sigma_1 \cos m\theta + \sigma_2 \sin m\theta)(\sigma_1 \cos m\theta' + \sigma_2 \sin m\theta') \quad (150)$$

In effect, S_2 is the same as R , except for the fact that (i) only a single Fermi liquid channel contributes, and (ii) there is an extra sum over μ , which was not present in R . The self-averaging of S_2 follows the same lines as above. Because of the extra sum (and the factor of g^2 in front) the ensemble average $\langle\langle S_2 \rangle\rangle$ is of order g^2 . Considering the same random-walk argument for $S_2 - \langle\langle S_2 \rangle\rangle$ we have four sums (g^4 steps in the random walk) with each step being of order $1/g^3$, and an additional factor of g^2 in front, leading to

$$\left(S_2 - \langle\langle S_2 \rangle\rangle \right) \simeq g^2 \frac{\sqrt{g^4}}{g^3} \simeq g \ll \left(\langle\langle S_2 \rangle\rangle \right) \quad (151)$$

Thus the fluctuations of S_2 are $1/g$ down from its self-average.

There is one subtlety with the effective action which is not present in the RG equation. The denominators of the RG equation can never be smaller than Λ , while those of S_2 go all the way to the smallest gap near the

Fermi energy. In the GOE the ensemble average $\ll S_2^2 \gg$ formally diverges due to the linear behavior of the level spacing distribution for small spacings. This implies that while the distribution for S_2 is sharply peaked around its average, it also has a long tail, which implies that the critical coupling u_m^* has a long tail as well. Calling the change in the critical coupling δu^* , and taking only the smallest level spacing into account, we find the tail to be

$$p_{tail}(\delta u^*) \approx 1/g^2(\delta u^*)^3 \quad (152)$$

This has the consequence that even systems nominally in the weak-coupling regime may occasionally be in the strong-coupling regime, with a probability that goes as $1/g^2(\delta u^*)^2$. Considering a system at $r_s = 5$, with $\Phi_2 = -0.25$, we have $\delta u^* = 3.279$. Assuming $g = 5$ we have a probability of 0.0037 of the system being in the strong-coupling phase.

VIII. APPENDIX B

Consider a generic theory with a fermion and a boson (ψ and σ in our problem), in which we integrate out the fermions to get an effective action S_{eff} for σ . It is clear that this action gives all the answers for questions involving σ alone. However, if at this stage we want to ask a question involving the fermions, which have been integrated out, how should one proceed? This is not an unprecedented situation, but we discuss it nonetheless for completeness.

Consider the following schematic partition function in which the fermions have been coupled to fermionic sources J, \bar{J} to enable a computation of their correlators:

$$Z(J, \bar{J}) = \int d\sigma d\psi d\bar{\psi} e^S \quad (153)$$

$$S(\sigma, \psi, \bar{\psi}) = \bar{J}\psi + J\bar{\psi} + \bar{\psi}(\partial + M\sigma)\psi - \sigma^2/2 \quad (154)$$

where M is a coupling matrix, and ∂ denotes the fermion kinetic energy. (In our case ($\partial = i\omega - \varepsilon_\alpha$)).

Upon integrating the fermions out we get

$$S_{eff}(\sigma) = \bar{J} \frac{1}{\partial + M\sigma} J + Tr \ln(\partial + M\sigma) - \sigma^2/2. \quad (155)$$

To obtain the fermion propagator G , we take the J and \bar{J} derivatives of $\ln Z$, set $J = \bar{J} = 0$, and obtain

$$G = (Z(0,0))^{-1} \int d\sigma \frac{1}{\partial + M\sigma} e^{S_{eff}(\sigma)}. \quad (156)$$

Thus the full G is just the propagator in a given external field σ , functionally averaged over σ with its effective action in the Boltzmann factor.

Let S_{eff} have the following expansion about a saddlepoint:

$$S_{eff} = S_0(\sigma_0) + \frac{1}{2} \delta\sigma D^{-1}(\sigma_0) \delta\sigma + \text{neglected terms} \quad (157)$$

If we ignore the fluctuations we get

$$G_{SP} = \frac{1}{\partial + M\sigma_0} \quad (158)$$

If we keep the gaussian fluctuations, we get to lowest nontrivial order

$$G = \frac{1}{\partial + M\sigma_0} \left[1 + \frac{1}{2} M \frac{1}{\partial + M\sigma_0} M \frac{1}{\partial + M\sigma_0} \langle \delta\sigma \delta\sigma \rangle + \dots \right] \quad (159)$$

where the average

$$\langle \delta\sigma \delta\sigma \rangle = D(\sigma_0) \quad (160)$$

is just the σ propagator in the gaussian approximation. Clearly, this procedure generates all the Feynman diagrams containing the three-point vertex coupling the fermions to fluctuations of σ . This series can be resummed in the usual way by constructing a self-energy for the fermions, with the lowest nontrivial contribution to it being Fig. 15. Thus there is no double-counting involved in using Fig. 15 (or Eq. (122)).

In the weak-coupling regime, $\sigma_0 = 0$, and Eq. (121) gives the inverse σ propagator. In the symmetry-broken strong-coupling regime, the term $\partial + M\sigma_0$ corresponds to the hamiltonian of Eqn. (130), the treatment of which follows the equation.

¹ V. M. Pudalov, M. D'Iorio, S. V. Kravchenko, and J. W. Campbell, Phys. Rev. Lett. **70**, 1866 (1993).

² For reviews see, Y. Imry, *Introduction to Mesoscopic Physics*, Oxford University Press, 1997; K. B. Efetov, *Supersymmetry in Disorder and Chaos*, Cambridge University Press, 1997.

³ D. V. Averin and K. K. Likharev, in *Mesoscopic Phenomena in Solids*, edited by B. L. Altshuler, P. A. Lee, and R. Webb (Elsevier, Amsterdam, 1991); C. W. J. Beenakker, Phys. Rev. B **44**, 1646 (1991).

⁴ For recent reviews, see, T. Guhr, A. Müller-Groeling, and H. A. Weidenmüller, Phys. Rep. **299**, 189 (1998); Y. Alhassid, Rev. Mod. Phys. **72**, 895 (2000); A. D. Mirlin, Phys. Rep. **326**, 259 (2000).

⁵ U. Sivan *et al*, Phys. Rev. Lett. **77**, 1123 (1996); S. R. Patel *et al*, Phys. Rev. Lett. **80**, 4522 (1998).

⁶ F. Simmel *et al*, Phys. Rev. B **59**, 10441 (1999); D. Abusch-Magder *et al*, Physica E **6**, 382 (2000).

⁷ F. Simmel, T. Heinzl, and D. A. Wharam, Eur. Lett. **38**, 123 (1997); J. A. Folk *et al*, Phys. Rev. Lett. **86**, 2102 (2001); S. Lüscher *et al*, Phys. Rev. Lett. **86**, 2118 (2001).

⁸ L. P. Levy, G. Dolan, J. Dunsmuir, and H. Bouchiat, Phys. Rev. Lett. **64**, 2074 (1990); V. Chandrasekhar, R. A. Webb, M. J. Brady, M. B. Ketchen, W. J. Gallagher, and A. Kleinsasser, Phys. Rev. Lett. **67**, 3578 (1991); D. Maily, C. Chapelier, and A. Benoit, Phys. Rev. Lett. **70**, 2020 (1993); Bertrand Reulet, Michel Ramin, Helene Bouchiat, and Dominique Maily, Phys. Rev. Lett. **75**, 124 (1995); E. M. Q.

- Jariwala, P. Mohanty, M. B. Ketchen, and R. A. Webb, Phys. Rev. Lett. **86**, 1594 (2001); R. Deblock, Y. Noat, B. Reulet, H. Bouchiat, and D. Mailly, Phys. Rev. B **65**, 075301 (2002); R. Deblock, R. Bel, B. Reulet, H. Bouchiat, and D. Mailly, Phys. Rev. Lett. **89**, 206803 (2002).
- ⁹ G. Murthy and H. Mathur, Phys. Rev. Lett. **89**, 126804 (2002).
- ¹⁰ G. Murthy and R. Shankar, Phys. Rev. Lett. **90**, 066801 (2003).
- ¹¹ D. Herman, H. Mathur, G. Murthy, and R. Shankar, in preparation.
- ¹² D. Herman, H. Mathur, and G. Murthy, cond-mat/0305364.
- ¹³ O. Bohigas, M. J. Giannoni, and C. Schmit, Phys. Rev. Lett. **52**, 1 (1984).
- ¹⁴ M. L. Mehta, *Random Matrices*, Academic Press, San Diego, 1991.
- ¹⁵ K. B. Efetov, Adv. Phys. **32**, 53 (1983); B. L. Altshuler and B. I. Shklovskii, Sov. Phys. JETP **64**, 127 (1986).
- ¹⁶ See, for example, V. R. Kogan and K. B. Efetov, cond-mat/0211258, and references therein.
- ¹⁷ R. Berkovits, Phys. Rev. Lett. **81**, 2128 (1998).
- ¹⁸ A. Cohen, K. Richter, and R. Berkovits, Phys. Rev. B **60**, 2536 (1999); P. N. Walker, G. Montambaux, and Y. Gefen, *ibid.*, 2541 (1999); S. Levit and D. Orgad, Phys. Rev. B **60**, 5549 (1999); D. Ullmo and H. U. Baranger, Phys. Rev. B **64**, 245324 (2001); V. Belinicher, E. Ginossar, and S. Levit, cond-mat/0109005; Y. Alhassid and S. Malhotra, Phys. Rev. B **66**, 245313 (2002).
- ¹⁹ J. B. French and S. S. M. Wong, Phys. Lett. **33B**, 447 (1970); O. Bohigas and J. Flores, Phys. Lett. **34B**, 261 (1971); Ph. Jacquod and A. D. Stone, Phys. Rev. Lett. **84**, 3938 (2000); Phys. Rev. B **64**, 214416 (2001); Y. Alhassid, Ph. Jacquod, and A. Wobst, Phys. Rev. B **61**, 13357 (2000); Physica E **9**, 393 (2001); Y. Alhassid and A. Wobst, Phys. Rev. B **65**, 041304 (2002).
- ²⁰ A. V. Andreev and A. Kamenev, Phys. Rev. Lett. **81**, 3199 (1998); P. W. Brouwer, Y. Oreg, and B. I. Halperin, Phys. Rev. B **60**, R13977 (1999); H. U. Baranger, D. Ullmo, and L. I. Glazman, Phys. Rev. B **61**, R2425 (2000); I. L. Kurland, I. L. Aleiner, and B. L. Altshuler, Phys. Rev. B **62**, 14886 (2000).
- ²¹ I. L. Aleiner, P. W. Brouwer, and L. I. Glazman, Phys. Rep. **358**, 309 (2002), and references therein; Y. Oreg, P. W. Brouwer, X. Waintal, and B. I. Halperin, cond-mat/0109541, and references therein.
- ²² G. Usaj, and H. U. Baranger, Phys. Rev. B **64**, 201319 (2001); cond-mat/0203074.
- ²³ G. Usaj and H. U. Baranger, Phys. Rev. B **67**, 121308 (2003).
- ²⁴ Y. Alhassid, T. Rupp, A. Kaminski, and L. I. Glazman, cond-mat/0212072; Y. Alhassid and T. Rupp, cond-mat/0212126.
- ²⁵ L. D. Landau, Sov. Phys. JETP **3**, 920 (1956); Sov. Phys. JETP **5**, 101 (1957).
- ²⁶ A. A. Abrikosov, L. P. Gorkov, and I. E. Dzyaloshinski, *Methods of Quantum Field Theory in Statistical Physics*, Dover Publications, New York, 1963.
- ²⁷ I. I. Pomeranchuk, Sov. Phys. JETP **8**, 361 (1958).
- ²⁸ R. Shankar, *Physica A* **177**, 530 (1991); R. Shankar, Rev. Mod. Phys. **66**, 129 (1994).
- ²⁹ B. L. Altshuler and A. G. Aronov, Sov. Phys. JETP **50**, 968 (1979); B. L. Altshuler, A. G. Aronov, and P. A. Lee, Phys. Rev. Lett. **44**, 1288 (1980); E. Abrahams, P. W. Anderson, P. A. Lee, and T. V. Ramakrishnan, Phys. Rev. B **24**, 6783 (1981).
- ³⁰ T. Tokuyasu, M. Kamal, and G. Murthy, Phys. Rev. Lett. **71**, 4202 (1993); N. Berdenis and G. Murthy, Phys. Rev. B **52**, 3083 (1995); G. Murthy and S. Kais, Chem. Phys. Lett. **290**, 199 (1998).
- ³¹ S. Chakravarty, B. I. Halperin, and D. R. Nelson, Phys. Rev. Lett. **60**, 1057 (1988); Phys. Rev. B **39**, 2344 (1989); For a detailed treatment of the generality of the phenomenon, see, S. Sachdev, *Quantum Phase Transitions*, Cambridge University Press, Cambridge 1999.
- ³² V. Ambegaokar and U. Eckern, Phys. Rev. Lett. **65**, 381 (1990); Phys. Rev. Lett. **67**, 3192 (1991); Europhys. Lett. **13**, 733 (1990); U. Eckern and A. Schmid, Europhys. Lett. **18**, 457 (1992).
- ³³ U. Eckern and P. Schwab, J. Low Temp. Phys. **126**, 1291 (2002).
- ³⁴ A. O. Caldeira and A. J. Leggett, Phys. Rev. Lett. **46**, 211 (1981).
- ³⁵ S. Chakravarty, Phys. Rev. Lett. **49**, 681 (1982).
- ³⁶ A. J. Bray and M. A. Moore, Phys. Rev. Lett. **49**, 1545 (1982).
- ³⁷ B. L. Altshuler, Y. Gefen, A. Kamenev, and L. S. Levitov, Phys. Rev. Lett. **78**, 2803 (1997).
- ³⁸ B. Georgeot and D. L. Shepelyansky, Phys. Rev. Lett. **79**, 4365 (1997); A. D. Mirlin and Y. V. Fyodorov, Phys. Rev. B **56**, 13393 (1997); P. G. Silvestrov, Phys. Rev. Lett. **79**, 3994 (1997); V. V. Flambaum and F. M. Izrailev, Phys. Rev. E **56**, 5144 (1997); C. Mejia-Monasterio, J. Richert, T. Rupp, and H. A. Weidenmüller, Phys. Rev. Lett. **81**, 5189 (1998); X. Leyonras, J. Tworzydło, and C. W. J. Beenakker, Phys. Rev. Lett. **82**, 4894 (1999); V. V. Flambaum and F. M. Izrailev, Phys. Rev. E **61**, 2539 (2000).
- ³⁹ R. A. Jalabert, A. D. Stone, and Y. Alhassid, Phys. Rev. Lett. **68**, 3468 (1992).
- ⁴⁰ A. M. Chang, H. U. Baranger, L. N. Pfeiffer, K. W. West, and T. Y. Chang, Phys. Rev. Lett. **76**, 1695 (1996); J. A. Folk, S. R. Patel, S. F. Godjin, A. G. Huibers, S. M. Cronenwett, and C. M. Marcus, Phys. Rev. Lett. **76**, 1699 (1996).
- ⁴¹ D. Pines and P. Nozieres, *The Theory of Quantum Liquids*, Addison-Wesley, Reading, MA 1989.
- ⁴² Y. Kwon, D. M. Ceperley, and R. M. Martin, Phys. Rev. B **50**, 1684 (1994).
- ⁴³ C. M. Varma, Phys. Rev. Lett. **83**, 3538 (1999).
- ⁴⁴ V. Oganesyan, S. A. Kivelson, and E. Fradkin, Phys. Rev. B **64**, 195109 (2001).
- ⁴⁵ A. M. Finkel'shtein, *Sov. Phys. JETP* **57**, 97 (1983); C. Castellani, C. Di Castro, P. A. Lee, and M. Ma, Phys. Rev. B **30**, 527 (1984).
- ⁴⁶ For a review of the theory, see, D. Belitz and T. R. Kirkpatrick, Rev. Mod. Phys. **66**, 261 (1994).
- ⁴⁷ D. Belitz and T. R. Kirkpatrick, Phys. Rev. B **53**, 14364 (1996); C. de C. Chamon and E. Mucciolo, Phys. Rev. Lett. **85**, 5607 (2000); C. Nayak and X. Yang, cond-mat/0302503.
- ⁴⁸ D. J. Gross and A. Neveu, Phys. Rev. D **10**, 3235 (1974).
- ⁴⁹ N. D. Mermin and H. Wagner, Phys. Rev. Lett. **17**, 1133 (1966); P. C. Hohenberg, Phys. Rev. **158**, 383 (1967).
- ⁵⁰ S. R. Patel, D. R. Stewart, C. M. Marcus, M. Gokcedag,

- Y. Alhassid, A. D. Stone, C. I. Duruoz, and J. S. Harris, Phys. Rev. Lett. **81**, 5900 (1998).
- ⁵¹ N. C. Byers and C. N. Yang, Phys. Rev. Lett. **7**, 46 (1961); F. Bloch, Phys. Rev. B **2**, 109 (1970); M. Buttiker, Y. Imry, and R. Landauer, Phys. Lett. A **96**, 365 (1983); H.-K. Cheung, E. K. Riedel and Y. Gefen, Phys. Rev. Lett. **62**, 587 (1989); A. Schmid, Phys. Rev. Lett. **66**, 80 (1991); F. von Oppen and E. K. Riedel, Phys. Rev. Lett. **66**, 84 (1991); B. L. Altshuler, Y. Gefen, and Y. Imry, Phys. Rev. Lett. **66**, 88 (1991).
- ⁵² H. Bouchiat and G. Montambaux, Jour. Phys. France **50**, 2695 (1989); G. Montambaux, H. Bouchiat, D. Sigeti, and R. Friesner, Phys. Rev. B **42**, 7647 (1990); M. Abraham and R. Berkovits, Phys. Rev. Lett. **70**, 1509 (1993); G. Bouzerar, D. Poilblanc, and G. Montambaux, Phys. Rev. B **49**, 8258 (1994); H. Kato and D. Yoshioka, Phys. Rev. B **50**, 4943 (1994); T. Giamarchi and B. S. Shastry, Phys. Rev. B **51**, 10915 (1995); P. Schmitteckert, R. A. Jalabert, D. Weinmann, and J. -L. Pichard, Phys. Rev. Lett. **81**, 2308 (1998); R. Berkovits and Y. Avishai, Phys. Rev. B **57**, R15076 (1998).
- ⁵³ V. E. Kravtsov and B. L. Altshuler, Phys. Rev. Lett. **84**, 3394 (2000).
- ⁵⁴ M. Schechter, Y. Oreg, Y. Imry, and Y. Levinson, Phys. Rev. Lett. **90**, 026805 (2003).
- ⁵⁵ P. W. Anderson, G. Yuval, and D. R. Hamann, Phys. Rev. B **1**, 4464 (1976). For full details, see, A. C. Hewson, *The Kondo Problem to Heavy Fermions*, Cambridge University Press, Cambridge, U.K., 1993.
- ⁵⁶ V. Ambegaokar, U. Eckern, and G. Schön, Phys. Rev. Lett. **48**, 1745 (1982).
- ⁵⁷ L. I. Glazman and K. A. Matveev, Sov. Phys. JETP **71**, 1031 (1990); K. A. Matveev, Sov. Phys. JETP **72**, 892 (1991).
- ⁵⁸ D. Goldhaber-Gordon, H. Shtrikman, D. Mahalu, D. Abusch-Magder, U. Meirav, and M. A. Kastner, Nature **391**, 156 (1998); S. M. Cronenwett, T. H. Osterkamp, and L. P. Kouwenhoven, Science **281**, 540 (1998).
- ⁵⁹ E. B. Kolomeisky, R. M. Konik, and X. Qi, Phys. Rev. B **66**, 075318 (2002).
- ⁶⁰ U. Sivan, F. P. Milliken, K. Milkove, S. Rishton, Y. Lee, J. M. Hong, V. Boegli, D. Kern, and M. DeFranza, Europhys. Lett. **25**, 605 (1994); U. Sivan, Y. Imry, and A. G. Aronov, Europhys. Lett. **28**, 115 (1994); D. R. Stewart, D. Sprinzak, C. M. Marcus, C. I. Duruoz, and J. S. Harris Jr., Science **278**, 1784 (1997).
- ⁶¹ A. Szafer and B. L. Altshuler, Phys. Rev. Lett. **70**, 587 (1993); B. D. Simons and B. L. Altshuler, Phys. Rev. B **48**, 5422 (1993).
- ⁶² R. O. Vallejos, C. H. Lewenkopf, and Y. Gefen, Phys. Rev. B **65**, 085309 (2002).
- ⁶³ R. Berkovits and Y. Avishai, Phys. Rev. Lett. **80**, 568 (1998).
- ⁶⁴ T. Rupp, Y. Alhassid, and S. Malhotra, Phys. Rev. B **65**, 193304 (2002).
- ⁶⁵ Y. Alhassid and A. Wobst, Phys. Rev. B **65**, 041304 (2002).
- ⁶⁶ K. Held, E. Eisenberg, and B. L. Altshuler, cond-mat/0208177.
- ⁶⁷ Y. Meir and N. S. Wingreen, Phys. Rev. Lett. **68**, 2512 (1992).
- ⁶⁸ P. N. Walker, Y. Gefen, and G. Montambaux, Phys. Rev. Lett. **82**, 5329 (1999); K.-H. Ahn, K. Richter, and I.-H. Lee, Phys. Rev. Lett. **83**, 4144 (1999).
- ⁶⁹ A. A. Koulakov, F. G. Pikus, and B. I. Shklovskii, Phys. Rev. B **55**, 9223 (1997); A. A. Koulakov and B. I. Shklovskii, Phys. Rev. B **57**, 2352 (1998); Phil. Mag. **B77**, 1235 (1998).
- ⁷⁰ M. A. Kastner, private communication.
- ⁷¹ H. U. Baranger and D. Ullmo, private communication.
- ⁷² W. B. Thimm, J. Kroha, and J. von Delft, Phys. Rev. Lett. **82**, 2143 (1999); I. Affleck and P. Simon, Phys. Rev. Lett. **86**, 2854 (2001); P. Simon and I. Affleck, Phys. Rev. B **64**, 085308; Phys. Rev. Lett. **89**, 206602 (2002); P. S. Cornaglia and C. A. Balsiero, Phys. Rev. B **66**, 115303 (2002).
- ⁷³ T. Senthil, M. P. A. Fisher, L. Balents, and C. Nayak, Phys. Rev. Lett. **81**, 4704 (1998).
- ⁷⁴ M. R. Zirnbauer, J. Math. Phys. **37**, 4986 (1996).